9. NEOGENE DIATOM BIOSTRATIGRAPHY, TEPHRA STRATIGRAPHY, AND CHRONOLOGY OF ODP HOLE 1138A, KERGUELEN PLATEAU[1]

Steven M. Bohaty,[2] Sherwood W. Wise Jr.,[3] Robert A. Duncan,[4] C. Leah Moore,[5] and Paul J. Wallace[6]

[2] Earth Sciences Department, University of California, Santa Cruz, Santa Cruz CA 95064, USA. **sbohaty@es.ucsc.edu**
[3] Department of Geological Sciences, 4100, Florida State University, Tallahassee FL 32306-4100, USA.
[4] College of Oceanic and Atmospheric Sciences, Oceanography Administration Building 104, Oregon State University, Corvallis OR 97331, USA.
[5] Earth and Land Science, University of Canberra, Canberra ACT 2601, Australia.
[6] Department of Geological Sciences, University of Oregon, Eugene OR 97403, USA.

ABSTRACT

A thick Neogene section was recovered in the upper ~300 m of Ocean Drilling Program Hole 1138A, drilled on the Central Kerguelen Plateau in the Indian sector of the Southern Ocean. Sediment lithologies consist primarily of mixed carbonate and biosiliceous clays and oozes, with several thin (1–3 cm) tephra horizons. The tephras are glass rich, well sorted, and dominantly trachytic to rhyolitic in composition. Volcaniclastic material in these horizons is interpreted to have originated from Heard Island, 180 km northwest of Site 1138, and was likely emplaced through both primary ash fall and turbiditic, submarine flows.

A Neogene age-depth model for Hole 1138A is constructed primarily from 36 diatom biostratigraphic datums. Nannofossil and planktonic foraminifer biostratigraphy provides supporting age information. Additionally, four high-precision ^{40}Ar-^{39}Ar ages are derived from ash and tephra horizons, and these radiometric ages are in close agreement with the biostratigraphic ages. The integrated age-depth model reveals a reasonably complete lower Miocene to upper Pleistocene section in Hole 1138A, with the exception of a ~1-m.y. hiatus at the Miocene/Pliocene boundary. Another possible hiatus is also identified at the Oligocene/Miocene boundary. High Neogene sedimentation rates and the presence of both calcareous and siliceous microfossils, combined with datable tephra horizons, establish Site 1138 as a suitable target for future drilling legs with paleoceanographic objectives. This report also pro-

poses two new diatom species, *Fragilariopsis heardensis* and *Azpeitia har-woodii,* from Pliocene strata of Hole 1138A.

INTRODUCTION

Eight sites were drilled on the Kerguelen Plateau and Broken Ridge during Ocean Drilling Program (ODP) Leg 183 from December 1998 to February 1999. Although the primary objective of the cruise was focused on the igneous history of the province, the overlying Cretaceous and Cenozoic sediments were also recovered in the course of operations. Several studies on these sediment sections are aimed at building on the regional biostratigraphic and paleoceanographic databases and adding information to that derived from Deep Sea Drilling Project (DSDP) Leg 26 and ODP Legs 119, 120, and 121 in the same area.

Hole 1138A was drilled on the Central Kerguelen Plateau (53°33′S, 75°58′E) in a water depth of 1141.4 m. The site is located south of the modern Polar Frontal Zone (PFZ) and ~180 km southeast of Heard Island (Fig. F1). Hole 1138A penetrated ~700 m of upper Neogene through Upper Cretaceous sediment and ~143 m of Cretaceous basement to a maximum depth of 842.70 meters below seafloor (mbsf). The sediment directly overlying subaerially erupted lava flows is assigned a Turonian age (~90 Ma) from nannofossil and planktonic foraminifer biostratigraphy (Coffin, Frey, Wallace, et al., 2000). The entire section in Hole 1138A was drilled with a rotary core barrel system and, therefore, only marginal recovery was achieved in some intervals. However, considering that the soft oozes of this section were rotary drilled, recovery is surprisingly high in Cores 183-1138A-13R through 1R (~77%), compared to ~49% for the entire sedimentary section. Most cores, though, show signs of drilling disturbance (Coffin, Frey, Wallace, et al., 2000).

The sediments recovered in Hole 1138A are divided into nine primary lithologic units and subunits (Coffin, Frey, Wallace, et al., 2000). The Neogene section ranges from Core 183-1138A-32R through 1R and includes lithostratigraphic Unit I, Subunits IIA and IIB, and the upper part of Subunit IIIA (Fig. F2). Unit I (0.0–112.0 mbsf) consists of foraminifer-bearing diatom clay and ooze. Subunits IIA and IIB (112.0–265.9 mbsf) are composed of foraminifer-bearing nannofossil clay and ooze. Several tephra horizons and intervals containing dispersed ash were also identified within Units I and II. Subunit IIIA (265.9–496.40 mbsf) is a foraminifer-bearing nannofossil chalk.

This report provides biostratigraphic information to supplement and expand on the diatom data originally presented in the shipboard report for Hole 1138A (Coffin, Frey, Wallace, et al., 2000). In addition to a biostratigraphic survey of diatoms, this study is also aimed at documenting Neogene tephra layers recovered in the hole and providing a summary of age-depth information. The age model derived here will assist in the limited paleoceanographic studies currently in progress, and, ultimately, these data will also aid in planning future drilling on the Central Kerguelen Plateau. Additional diatom results from Leg 183 are reported by Arney et al. (this volume) for Hole 1140A, located on the Northern Kerguelen Plateau. Their zonal scheme and taxonomy, however, differ slightly from those presented here (see "Systematic Paleontology," p. 15, for general notes on the taxonomy applied to diatom assemblages from Hole 1138A).

The nearest comparable section to Hole 1138A previously drilled on the Central Kerguelen Plateau is ODP Hole 747A (Leg 120), located 150

F1. Locations of ODP Sites 747 and 1138, p. 35.
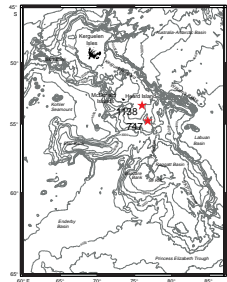
F2. Neogene tephra horizons and diatom and nannofossil abundance, p. 36.

S.M. Bohaty et al.
Neogene Diatom and Tephra Stratigraphy

3
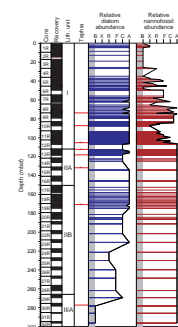
km southeast of Site 1138 (54°49′S, 76°48′E) in a water depth of 1695.0 m (Fig. F1). Diatom biostratigraphy for Hole 747A is reported in Harwood and Maruyama (1992). The diatom record and biochronology of these two holes are compared below.

METHODS

Diatom Preparation

Samples from Hole 1138A were prepared for diatom analysis using standard procedures. Two preparations were made for each sample, including an unprocessed or "raw" preparation and a processed preparation. Two subsamples (~0.25 g) for each interval were placed in 15-mL centrifuge tubes. One set of subsamples was disaggregated in deionized water, and the other was chemically treated. The treated samples were initially reacted with ~5 mL of 10% hydrochloric acid in order to remove the carbonate component. The centrifuge tubes were shaken on a vortex stirrer and then set aside to react for 1 hr. Following these steps, ~3 mL of 30% hydrogen peroxide was added to remove organic material and help disaggregate biosiliceous "clumps." The samples were soaked overnight in the HCl/H_2O_2 solution and then thoroughly washed by centrifuging three times at ~1500 rpm for 10 min. The samples were not heated during chemical treatment.

Strewn slides of all samples for diatom analysis were made on 20-mm × 40-mm coverslips. Each centrifuge tube was filled with ~8 mL of deionized water and then mixed on a vortex stirrer. After settling for 30 s to let the sand-sized fraction settle out, a small aliquot was removed from the center of the suspension with a pipette. Two or three drops of sample were then pipetted onto a coverslip containing a thin film of deionized water. All samples were mounted in Norland optical adhesive 61 (refractive index [RI] = 1.56). A few selected samples for photomicrography were sieved to obtain a >10-μm fraction (using nylon screens) and mounted in Naphrax (RI = 1.74).

Because of low-to-moderate core recovery in the Miocene section of Hole 1138A, only core catcher samples were examined for Cores 183-1138A-32R through 15R. Above this level, many discrete core samples were examined in addition to the core catcher sample. A full sample list is given in the left column of Table T1.

Relative diatom abundance was determined from strewn slides of the unsieved, chemically treated (HCl and H_2O_2) preparations. The total relative abundance of diatoms (as a group) was determined at 600× magnification and was based on the average number of specimens observed per field of view. Several traverses were made across the coverslips, and abundance estimates were recorded (Table T1; Fig. F2) as follows:

A = abundant (>10 valves per field of view).
C = common (3–9 valves per field of view).
F = few (1–2 valve(s) per field of view).
R = rare (1 valve in 2–30 fields of view).
T = trace (very rare fragments present).
B = barren (no diatom valves or fragments present).

The qualitative abundance of individual diatom taxa in Hole 1138A (Table T1) is based on the approximate number of specimens observed per field of view at 1000×. Individual species abundance categories are

S.M. Bohaty et al.
Neogene Diatom and Tephra Stratigraphy

4

listed below. Generally, one-quarter to one-half of the 20-mm × 40-mm coverslip was examined (40 mm = ~200 fields of view). After initial abundance determinations were made at 1000×, the slides were then routinely scanned at 600× to identify rare taxa.

A = abundant (≥2 valves per field of view).
C = common (1–5 valve(s) in 5 fields of view).
F = few (~1–3 valve(s) in 20 fields of view).
R = rare (~1–2 valve(s) in 60 fields of view).
X = present (≤1 valve or identifiable fragment per traverse of coverslip).
r = rare occurrences of a taxon interpreted as reworked specimens.
d = rare occurrences of a taxon interpreted as downcore contamination.

The degree of siliceous microfossil fragmentation often mirrors dissolution, but the two factors are not necessarily dependent (i.e., well-preserved samples can be highly fragmented). Preservation of diatoms, therefore, was qualitatively based on the degree of dissolution and was rated as follows:

G = good (slight to no dissolution).
M = moderate (moderate dissolution).
P = poor (severe effects of dissolution).

In addition to diatoms, the relative abundance of a few ebridian and endoskeletal dinoflagellate taxa was also noted (Table T1). The stratigraphic distribution of silicoflagellates in the Neogene section of Hole 1138A is treated in a separate chapter in this volume (**McCartney et al., this volume**).

To compare with diatom abundance, the relative abundance of calcareous nannofossils was also noted in the "raw" sediment preparations (Table T1; Fig. F2). These estimates were made in cross-polarized light at 1000× using the qualitative abundance designations outlined by Wei and Wise (1992).

Tephra Preparation

Four tephra horizons were sampled for this study (Fig. F2). These samples were heated in dilute acetic acid to remove calcareous microfossils and then wet sieved to remove the <32-μm component, which was dominated by siliceous microfossil material. Glass shards from the tephra samples were examined by scanning electron microscopy (SEM), and ~70 shards were analyzed for major elements by electron probe using techniques described by Wallace (2002).

Radiometric Methods

Crystallization ages of glass shards and minerals in discrete ash layers were measured using the ^{40}Ar-^{39}Ar incremental heating method. The chief advantages of this technique over conventional K-Ar dating are in separating the contributions of primary igneous and secondary alteration phases to the total sample Ar composition and in identifying any initial, nonatmospheric Ar, if present. This is accomplished, after neutron irradiation, to produce ^{39}Ar from ^{39}K by heating the sample in in-

S.M. Bohaty et al.
Neogene Diatom and Tephra Stratigraphy

5

creasing temperature steps and analyzing the composition of Ar released at each step (e.g., Dalrymple et al., 1981; McDougall and Harrison, 1999). Crystallization ages are then interpreted from convergence of step ages toward a mid- to high-temperature plateau age and independently from the slope of collinear step compositions in Ar isotope ratio plots (i.e., an isochron age).

Experiments were run using both glass shards and biotites separated from the ash layers described in Coffin, Frey, Wallace, et al. (2000). Samples were selected for dating on the basis of examination under binocular microscope to assess shard morphology (size and vesicularity) and state of alteration of either glass or biotite grains. After handpicking to obtain 20–30 mg of material, separates were cleaned in dilute nitric acid followed by ultrasonic washing in distilled water. The samples were then wrapped in Cu foil, labeled, loaded in quartz vials, and interspaced with 10-mg aliquots of biotite monitor FCT-3 (28.04 ± 0.12 Ma; calibrated against Mmhb-1 hornblende at 523.5 Ma [Renne et al., 1994]). Quartz vials were evacuated, sealed in standard Al tubes, and irradiated for 6 hr at 1 MW power in the center ring of the TRIGA reactor at Oregon State University, Corvallis, Oregon.

FCT-3 biotite was placed at multiple vertical positions along the 80-mm center vial, which provided neutron flux measurements (J values) that varied smoothly within a ~10% range. Horizontal gradients in J values are known from previous experience to be <1%. J values for the sample positions were interpolated from a second-order polynomial fit to the monitors. Errors in sample J values (0.5%) accumulated from the individual monitor measurements and gradient fitting.

Ar isotopic compositions of samples were measured with a MAP-215/50 mass spectrometer connected to an ultra-high vacuum resistance furnace and Zr-Al getters. Samples were heated from 400°C to fusion in 50°–100°C increments. The system was operated in the peak-hopping mode (for m/z = 35, 36, 37, 38, 39, and 40) by computer. Peak decay is typically <10% for the MAP system, which has a measured sensitivity of 4×10^{-14} mol/V, and regressed peak heights against time follow linear fits. Mass discrimination on the MAP system was measured using zero-age basalt disks run in the same way as the samples and was constant at 1.005 (for 2 amu). The background for the mass spectrometer is 1.5×10^{-18} mol at m/z = 36, 2×10^{-18} mol at m/z = 39, and 1.5×10^{-16} mol at m/z = 40. Procedure blanks range from 3.0×10^{-18} mol ^{36}Ar and 5.4×10^{-16} mol ^{40}Ar at 600°C to 6.4×10^{-18} mol ^{36}Ar and 1.7×10^{-15} mol ^{40}Ar at 1400°C.

MICROFOSSIL OCCURRENCE

Siliceous microfossils are present in all samples from Cores 183-1138A-29R through 1R (269.41–0.0 mbsf) (Table T1). Diatoms, however, are poorly preserved and in generally low abundance in the interval between Cores 183-1138A-29R and 20R (269.41–181.30 mbsf); siliceous microfossils in this interval are clearly affected by dissolution. In contrast, moderate to good preservation and high diatom abundance characterizes Cores 183-1138A-19R through 1R (174.75–0.0 mbsf); the moderately preserved samples in this interval are predominantly affected by physical breakage. Nannofossils are abundant in Cores 183-1138A-36R through 13R (340.60–113.00 mbsf) and are present in variable abundance above this level (Cores 12R through 1R; 107.03–0.0 mbsf). A graphical representation of relative diatom and nannofossil

abundance is shown in Figure F2. The position of the horizontal bars in Figure F2 represents the sample depths examined in the present study.

The stratigraphic distribution of individual diatom, ebridian, and endoskeletal dinoflagellate taxa is recorded in Table T1. Abundant diatoms and moderate-to-good preservation in most samples allowed identification of continuous biostratigraphic ranges for most taxa. Some rare occurrences are attributed to limited reworking and downhole contamination (Table T1). Taxonomic and occurrence notes for diatom taxa identified in Hole 1138A are given in "Systematic Paleontology," p. 15, and several specimens are illustrated in Plates P1, P2, and P3. Two new diatom species, *Fragilariopsis heardensis* and *Azpeitia harwoodii,* are described from lower and upper Pliocene strata of Hole 1138A.
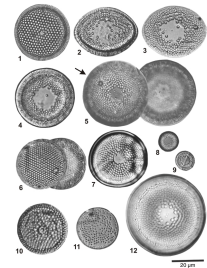
DIATOM ZONAL ASSIGNMENTS

The diatom zonal scheme applied to the Neogene section of Hole 1138A is modified from that proposed by Harwood and Maruyama (1992) (Fig. F3A, F3B). Published datum ages were adjusted to the Berggren et al. (1995) geomagnetic polarity timescale (GPTS), and some age calibrations were preferentially selected from sites on the Kerguelen Plateau. In the modified zonal scheme used here, the first occurrence (FO) of *Thalassiosira miocenica* is replaced by the FO of *Thalassiosira oliverana* as the base of the *Nitzschia reinholdii* Zone, following the convention set during Legs 178 (Barker, Camerlenghi, Acton, et al., 1999) and 188 (O'Brien, Cooper, Richter, et al., 2001). The published age for both of these datums is reported at 6.4 Ma. The FO of *T. oliverana,* however, has not been rigorously calibrated to the polarity timescale and is considered to be an approximate age. The modified *N. reinholdii* Zone used here is that of Harwood and Maruyama (1992) and not the original *N. reinholdii* Zone defined by Weaver and Gombos (1981); the *N. reinholdii* Zone of Weaver and Gombos (1981) utilizes the last abundant appearance datum (LAAD) of *Denticulopsis simonsenii* (synonymous with the former taxonomic usage of *Denticulopsis hustedtii*) as its base. We have also exchanged the FO of *Thalassiosira spumellaroides* (22.6 Ma) for the last occurrence (LO) of *Rocella gelida* (22.3 Ma) as the base of the *T. spumellaroides* Zone. In Leg 177 studies, the FO of *Thalassiosira vulnifica* was replaced by the FO of *Fragilariopsis weaveri* (Zielinski and Gersonde, 2002). We have not made this modification but are aware of possible diachronous occurrences for both the FO and LO of *T. vulnifica* in different regions of the Southern Ocean.

The names of several zones summarized and defined by Harwood and Maruyama (1992) have been changed to reflect recent taxonomic revisions. The former Pliocene–Pleistocene *Nitzschia* spp. zones have been changed to *Fragilariopsis* spp., following the taxonomy of Gersonde and Bárcena (1998). The names of the former *Nitzschia hustedtii*– *Nitzschia grossepunctata* and *N. hustedtii* Zones are also changed to the *D. simonsenii*–*N. grossepunctata* and *D. simonsenii* Zones, respectively, in order to reflect taxonomic clarifications in the *Denticulopsis* group by Yanagisawa and Akiba (1990).

A total of 23 single and combined diatom biozones are recognized in Hole 1138A (Tables T1, T2, T3). The datums used to define the Miocene diatom zones are listed in Table T2, and the Pliocene–Pleistocene zones are outlined in Table T3. The Pliocene–Pleistocene zones are better con-
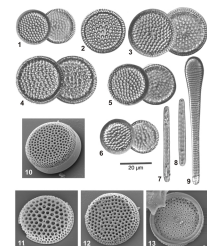
P1. *Thalassiosira* and *Actinocyclus* specimens, p. 50.
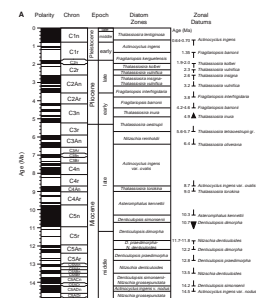

P2. *Fragilariopsis* specimens, p. 51.
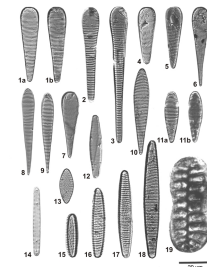
P3. *Azpeitia harwoodii*, p. 52.

F3. Diatom zonal scheme, p. 37.

T2. Miocene diatom zonal assignments, p. 44.

T3. Pliocene–Pleistocene diatom zonal assignments, p. 45.

S.M. Bohaty et al.
Neogene Diatom and Tephra Stratigraphy

7

strained because of a higher sampling frequency in the upper part of the Hole 1138A section.

Diatom biostratigraphy divides the Neogene section of Hole 1138A into well-defined time-rock units. A poorly preserved uppermost Oligocene–lowermost Miocene diatom assemblage is present in Sample 183-1138A-29R-CC (269.41 mbsf). Samples 183-1138A-28R-CC through 12R-3, 100–101 cm (261.81–106.30 mbsf), are assigned to the lower to upper Miocene; Samples 12R-2, 100–101 cm, through 7R-3, 25–26 cm (104.80–58.05 mbsf), are placed in the lower to upper Pliocene; and Samples 7R-2, 100–102 cm, through 1R-1, 70–71 cm (57.30–0.70 mbsf), are placed in the lower to upper Pleistocene (Tables T2, T3). Sub-epoch boundaries within the Miocene and Pliocene are also roughly defined based on diatom biostratigraphy (Tables T2, T3).

Several diatom zones could not be defined in Hole 1138A because of the absence or sporadic occurrence of marker taxa. These datums include the FO of *Crucidenticula kanayae* (the base of the *C. kanayae* Zone), the FO of *N. grossepunctata* (the base of the *N. grossepunctata* Zone), and the FO of *Asteromphalus kennettii* (the base of the *A. kennettii* Zone). The FOs of *Nitzschia denticuloides* and *D. simonsenii* are concurrent; thus, the *D. simonsenii–N. grossepunctata* Zone could not be defined. This is also the case for the FOs of *Thalassiosira torokina* and *Actinocyclus ingens* var. *ovalis,* which prevented recognition of the *T. torokina* Zone. These concurrent datums may be a result of low core recovery, large sampling intervals, or actual synchroneity of the datum events at this site.

TEPHRA MORPHOLOGY AND COMPOSITION

The tephra layers recovered from Hole 1138A (Fig. F2) are 1–3 cm thick, massive, and vary in color from light to dark gray. All four tephra layers sampled for this study are glass rich (95%–100% glass shards), crystal and lithic fragment poor, fine grained (mean grain size ranges from very fine to medium sand), and well sorted. Major element analyses yielded totals of 95.0 ± 2.4 wt%, suggesting the presence of ~5 wt% H_2O in the glass as a result of postemplacement low-temperature hydration. In grain mount, felsic shards are typically pale brown to translucent gray. Mafic shards tend to be blocky (vesicle poor) and yellowish brown in color. Small flakes of brown biotite are present in Samples 183-1138A-13R-1, 22–24 cm, and 19R-1, 110–112 cm, and most tephra layers contain minor plagioclase and/or sanidine.

The tephra from interval 183-1138A-12R-3, 5–7 cm (105.36 mbsf), (see Pl. P4, fig. 1) contains glass shards with a wide range of compositions, including basaltic trachyandesite, trachyandesite, trachyte, and rhyolite (Fig. F4). The mean grain size for the vitric concentrate is fine to medium sand (250 µm; 2.0 ɸ). Tube vesicular pumice (50%–60% vesicles) and elongate bubble wall shards are the principal components of the ash, but rare blocky mafic clasts have <10% vesicles. Mean grain size for these blocky shards is fine sand (200 µm; 2.25 ɸ).

The tephra from Section 183-1138A-13R-1, 22–24 cm (112.23 mbsf), contains glass shards that are dominantly trachyte in composition (Fig. F4). The mean grain size for the vitric concentrate is very fine sand (75 µm; 3.75 ɸ). The sample is composed of tube vesicular pumice (50%–60% vesicles) with brittle fractures subperpendicular to tube orientation.

The tephra from Section 183-1138A-15R-1, 73–75 cm (131.94 mbsf) (see Pl. P4, fig. 2), contains glass shards that vary from trachyte to rhyo-

P4. Glass shards in tephra layers, p. 53.
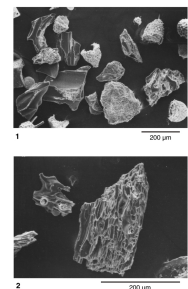
F4. Total alkalis vs. SiO_2 classification plot, p. 39.
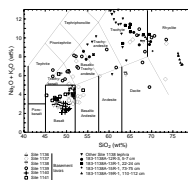
lite (Fig. F4). The mean grain size for the vitric concentrate is fine to medium sand (250 μm; 2.0 φ). The sample is composed of tube vesicular pumice (highly vesicular; 60%–70%) with abundant small tubes. Shard morphology is strongly vesicle controlled, with brittle fractures parallel and subperpendicular to tube orientation.

The tephra from interval 183-1138A-19R-1, 110–112 cm (170.81 mbsf), contains glass shards that are dominantly high-silica rhyolite in composition with less abundant trachyte shards (Fig. F4). The mean grain size for the vitric concentrate is medium sand (350 μm; 1.5 φ). The sample is composed of elongate tube vesicular to platey clasts with a few large tube vesicles. Less abundant, equant tricuspate shards and shards with spherical vesicles are also preserved.

The fine-grained, well-sorted, and massive nature of the tephras from Hole 1138A is consistent with deposition from a distal ash cloud or fines elutriated from a subaqueous flow and dispersed in the water column. In order for glass shard–rich massive tephra horizons up to 3 cm thick to be preserved in marine sediments, a considerable influx of volcaniclastic material is required. The tephras have a dominantly felsic composition, and high vesicularities indicate a large proportion of exsolved volatiles in the erupting magma. Eruption of gas-charged viscous felsic magma is typically highly explosive, and a large volume of ejecta is commonly dispersed over a large area, particularly downwind from the eruption (Cas and Wright, 1988). An alternative mechanism for dispersion of fine-grained, well-sorted ash into the water column is as a byproduct of the entry of pyroclastic flows into the sea, or the subsidence of volcaniclastic deposits into the sea, initiating subaqueous gravity flows (ash turbidites). The associated clouds of elutriated fines could settle and form deposits that would appear similar to those formed from primary fall activity.

Tephras preserved in marine sediments older than those considered in this study contain a greater proportion of mafic and blocky-shaped glass shards (Coffin, Frey, Wallace, et al., 2000). This pattern of evolution from mafic to more felsic compositions, and from clast morphologies reflecting interaction with water to morphologies that are more typical of subaerial eruption, reflects the general evolution of magmatism on the Kerguelen Plateau. The tephras sampled for this study are dominantly trachytic to rhyolitic in composition and are generally alkalic. When compared with basement lavas of the Kerguelen Plateau and volcanic rocks from Heard Island and the Kerguelen archipelago, compositions appear broadly similar (Fig. F4) (Coffin, Frey, Wallace, et al., 2000). The likely source for the tephra deposits at Site 1138 is Heard Island, located 180 km to the northwest. Bathymetric surveys indicate that a submarine canyon runs south of Heard Island and passes near Site 1138. This observation suggests that some ash sampled for this study may have been contributed from fines associated with subaqueous flows originating at Heard Island (Coffin, Frey, Wallace, et al., 2000), as well as from primary ash fall.

TEPHRACHRONOLOGY

Mass spectrometric data from tephra samples are summarized in Table T4 and presented graphically in Figure F5. Complete experimental data and plots are available in electronic files from the journal or on request from the authors. Fitted Ar isotopic ratios from step measurements are used in two ways. Assuming that initial sample Ar

T4. ^{40}Ar-^{39}Ar incremental heating ages, p. 47.

F5. Age plateau and isochron diagrams, p. 40.
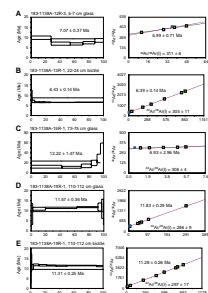
compositions were atmospheric (initial ^{40}Ar/^{36}Ar = 295.5), step ages are plotted against cumulative percent ^{39}Ar released, as age spectrum, or plateau diagrams. In addition, isotope correlation diagrams (^{40}Ar/^{36}Ar vs. ^{39}Ar/^{36}Ar) are examined for collinear step compositions; the slope is equivalent to age since closure, and the ^{40}Ar/^{36}Ar intercept reveals the initial Ar composition of the system (rock or mineral). We accept an apparent age as an accurate estimate of the sample crystallization age if several statistically testable conditions are met (Dalrymple et al., 1980; Pringle and Duncan, 1995), namely (1) a well-defined, mid- to high-temperature plateau is formed by at least three concordant, contiguous steps representing >50% of the ^{39}Ar released; (2) a well-defined isochron exists for the plateau step Ar compositions; (3) the plateau and isochron ages are concordant; and (4) the isochron ^{40}Ar/^{36}Ar intercept is atmospheric composition.

Most of the sample ages presented in Table T4 meet the criteria listed above. Total gas ages are calculated by recombining all steps from each sample and are roughly equivalent to conventional K-Ar ages. Plateau ages (2 σ uncertainties) are the mean of from three to eight step ages, representing >50% of the total sample ^{39}Ar, weighted by the inverse of variance. Sample 183-1138A-12R-3, 5–7 cm, glass (A1) produced a saddle-shaped age spectrum (Fig. F5A) with a three-step plateau and older ages at the lowest temperature and highest temperature steps, suggestive of small amounts of excess (nonatmospheric) ^{40}Ar trapped in the quenched glass at the time of crystallization. The corresponding three-step isochron produced a significantly younger age (5.99 ± 0.71 Ma) and an initial ^{40}Ar/^{36}Ar intercept greater than the atmospheric value (295.5). The isochron age is preferred because of the evidence for excess ^{40}Ar and because it fits stratigraphically with the much better resolved biotite age from Sample 183-1138A-13R-1, 22–24 cm (A2), in the underlying core. This second sample produced a tight plateau age (six of seven steps; 99% of the total gas released) and concordant isochron age (Fig. F5B). We accept this age as a reliable estimate of the eruption and immediate deposition events. Sample 183-1138A-15R-1, 73–75 cm, glass (A3) also showed evidence of undegassed, excess ^{40}Ar, in the form of old ages at high-temperature steps (Fig. F5C). The lowest three temperature steps produced a poorly resolved plateau, but the isochron based on all steps indicated a younger age and a nonatmospheric initial Ar composition. The isochron age, although imprecise, appears to be the better estimate of the age of crystallization and deposition of this ash layer. Two samples were analyzed from interval 183-1138A-19R-1, 110–112 cm, with compositions of glass (A5) (Fig. F5D) and biotite (A4) (Fig. F5E). These produced concordant plateau and isochron ages with atmospheric initial Ar compositions. We use the weighted mean of the isochron ages (11.45 ± 0.22 Ma) as the best estimate of the age of this horizon.

AGE MODEL AND SEDIMENTATION RATES

An age-depth model for the Neogene section of Hole 1138A (Fig. F6) is constructed from tephra ^{40}Ar-^{39}Ar ages (Table T4), biostratigraphic datums, and magnetostratigraphic tie points to the GPTS (Tables T5, T6; Fig. F6). The biostratigraphic age constraints are derived primarily from 36 diatom datums, but several planktonic foraminifer and nannofossil datums (Coffin, Frey, Wallace, et al., 2000) are also incorporated. The

F6. Neogene age-depth plot, p. 41.
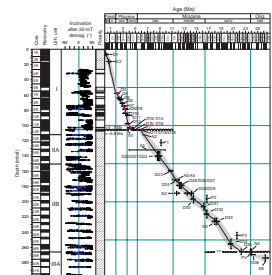
T5. Neogene biostratigraphic datums, p. 48.

T6. Paleomagnetic stratigraphy and ages, p. 49.

calibrated age for each diatom datum is compiled from the sources listed in the Table T5 caption. The age model for the Neogene section of Hole 1138A is interpreted in terms of possible error in the calibrated ages for the biostratigraphic datums (Fig. F6), and we apply a uniform ±300-k.y. error to all individual diatom (D), nannofossil (N), and planktonic foraminifer (P) datums. The line on Figure F6 represents a "best fit" age model, and the gray "envelope" represents an interpreted total uncertainty in the age model. The vertical error bars for the biostratigraphic datums (Fig. F6) reflect uncertainty in the datum depth intervals resulting from sample spacing gaps.

Three diatom zonal datums were not used in the construction of the age-depth plot for Hole 1138A. The FO of *T. oliverana* does not have a well-established age calibration, and there is also some taxonomic uncertainty associated with the identification of this taxon resulting from the presence of *T. oliverana* var. *sparsa,* which has a documented older/lower FO than *T. oliverana* s.s. (Harwood and Maruyama, 1992). *Thalassiosira insigna* is very rare in the upper part of its range, limiting its LO datum as a useful marker. Intermediate forms between *Fragilariopsis barronii* and *Fragilariopsis kerguelensis* are present in the upper part of the range of *Fragilariopsis barronii* (see Gersonde and Bárcena, 1998), which similarly inhibits accurate identification of the LO datum for *F. barronii.*

Four biostratigraphic datums fall outside the interpreted age envelope for Hole 1138A (Fig. F6). These include the FO of *Neogloboquadrina pachyderma* (P1), the LO of *Cyclicargolithus floridanus floridanus* (N2), the FO of *Globorotalia miozea* (P2), and the FO of *Paragloborotalia incognita* (P3). It is unclear why these datums are not consistent with the other age data. These inconsistencies may be a result of poorly calibrated ages in the southern high latitudes for nannofossils and planktonic foraminifers, sample spacing gaps, or problems with the diatom age calibrations. The coincidence of the LO of *C. floridanus floridanus* (N2) with diatom datums D28 and D29 (between ~191 and 186 mbsf) may indicate the presence of a middle Miocene hiatus. Well-constrained tephra ages A4 and A5 at ~171 mbsf, however, suggest the calibrated age for N2 is too young and that the middle Miocene interval is continuous.

Shipboard paleomagnetic analyses using a pass-through cryogenic magnetometer were performed on the entire sedimentary section recovered in Hole 1138A; stable and reliable inclination data were obtained after alternating-field demagnetization at 20 mT (Coffin, Frey, Wallace, et al., 2000). Although paleomagnetic data are available through the entire Neogene section, polarity reversal ties to the GPTS are only attempted in the Pliocene–Pleistocene interval. Poor recovery in the Miocene section significantly hinders paleomagnetic interpretation, particularly in intervals with many chrons of short duration (e.g., in the middle Miocene). In the Pliocene–Pleistocene section, diatom biostratigraphy provides sufficient time constraint for the recognition of Subchron C1r.1n, Chron C2n, and Subchrons C2An.1n, C2An.2n, and C3n.1n (Fig. F6; Table T6). Application of this preferred fit to the GPTS does not result in any significant inconsistencies with the biostratigraphic information. However, one exception is the placement of the top of Subchron C2An.1n. Assigning the normally polarized interval between 73.87 and 74.83 mbsf to C2An.1n requires an age assignment for the upper level (2.58 Ma at 74.83 mbsf) that is apparently too young. The reason for this inconsistency is unclear, as a hiatus does not appear to be present at this level.

Overall, a well-constrained Neogene age-depth model is derived from data compiled here for Hole 1138A. Additionally, there is excellent

agreement between the biostratigraphic and radiometric ages. A relatively expanded Neogene section is present in Hole 1138A. Sedimentation rates for the Miocene section (~265–105 mbsf) averaged ~10 m/m.y., and sedimentation rates in the lower Pliocene–upper Pleistocene section (~105–0.0 mbsf) averaged ~22 m/m.y.

Compiled age information for Hole 1138A identifies an uppermost Miocene–lowermost Pliocene disconformity between Sections 183-1138A-12R-2 and 12R-3 (Fig. F6). Diatom biostratigraphy and tephra age A1 indicate this hiatus spans the interval from ~4.7 to ~5.8–6.0 Ma. The maximum age range for the hiatus is derived from the truncation of the ranges for the diatoms *Nitzschia miocenica* (D19) and *Fragilariopsis donahuensis* (D18), both with LOs between 5.8 and 6.2 Ma. This interpretation is also supported by the absence of *Thalassiosira tetraoestrupii* (D17) in Section 183-1138A-12R-3 (FO = 5.7 Ma). An ash age of 5.99 ± 0.71 Ma (A1) at the top of Section 183-1138A-12R-3 corroborates the biostratigraphic age interpretation. A diatom sample immediately above the ash horizon (Sample 183-1138A-12R-2, 100–101 cm; 104.80 mbsf) contains *Thalassiosira complicata* (D15), indicating an age of ≤4.7 Ma. A color change is also evident in the shipboard photo of Core 183-1138A-12R. Section 183-1138A-12R-3 is slightly lighter colored than Section 12R-2 (Coffin, Frey, Wallace, et al., 2000), indicating a higher carbonate (nannofossil) content of upper Miocene sediments of Section 12R-3. Additionally, there is a magnetic polarity reversal (normal to reversed polarity in the upcore direction) between Samples 183-1138A-12R-3, 15 cm, and 12R-3, 10 cm (105.45–105.40 mbsf), further indicating the presence of a hiatus at this level.

Another possible hiatus or condensed section is present at the Oligocene/Miocene boundary between ~270 and 260 mbsf (Fig. F6). This interval of the drill core is not well constrained biostratigraphically, due to poor core recovery and low-resolution sampling. Biostratigraphic data indicate that a hiatus, if indeed present, spans the time interval between ~22.5 and 24.0 Ma.

DISCUSSION

The age-depth information summarized above indicates that a ~105-m-thick Pliocene–Pleistocene section and a ~165-m Miocene section are present in Hole 1138A (Fig. F6). Even though the lowermost Pliocene interval is missing, the lower Pliocene to upper Pleistocene section in Hole 1138A is one of the thickest recovered to date on the Kerguelen Plateau. The only comparable sections are those sections recovered during Leg 119 on the Northern Kerguelen Plateau at ODP Sites 736 and 737 and a deepwater section recovered on the Southern Kerguelen Plateau at Site 745 (Barron et al., 1991). The acquisition of a thick Quaternary section was a major objective of ODP Leg 120 (Sites 747–752); the designated Neogene site (751), however, yielded primarily Miocene rather than Pliocene–Pleistocene sediments (Schlich, Wise, et al., 1989).

Enhanced sedimentation rates through the Neogene at Site 1138 may, in part, be explained by the input of both ash and terrigenous clay material. A submarine canyon has been identified ~45 km west of Site 1138, and turbidity currents associated with this feature may have supplied distal overbank sediments to the site (Coffin, Frey, Wallace, et al., 2000). In addition to ash fall from periodic eruptions on Heard Island, this process may account for the expanded nature of Unit I and Subunit

S.M. Bohaty et al.
Neogene Diatom and Tephra Stratigraphy

12

IIA in Hole 1138A (upper Miocene and lower Pliocene through upper Pleistocene).

The nearest comparable Neogene section to that of Hole 1138A lies at Site 747, also on the Central Kerguelen Plateau (Fig. F1). Hole 747A contains a ~29-m Pliocene–Pleistocene section and a ~98-m Miocene section (Harwood and Maruyama, 1992; Harwood et al., 1992; Ramsay and Baldauf, 1999), indicating that the Pliocene–Pleistocene section in Hole 1138A is expanded relative to nearby Hole 747A. An upper Miocene–lowermost Pliocene disconformity is present in both drill cores. The hiatus within Hole 747A, however, spans a much longer time interval, from ~5 to 9 Ma (Harwood et al., 1992; Ramsay and Baldauf, 1999). An upper Miocene–lowermost Pliocene disconformity is a common feature of many cores drilled in the Southern Ocean (see Wise et al., 1985, fig. 7; Ramsay and Baldauf, 1999, fig. 60). This may be related to cooling and intensification of the Antarctic Circumpolar Current through the late Miocene–earliest Pliocene interval.
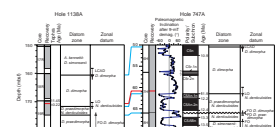
Harwood et al. (1992) identify a possible hiatus near the Oligocene/Miocene boundary in Hole 747A. Ramsay and Baldauf (1999), however, consider the polarity sequence through this interval of Hole 747A to be complete. This discrepancy arises from the assignment of chron designations, which are not well constrained with biostratigraphy and are ambiguous for this core interval. Regardless, the possible hiatus at the Oligocene/Miocene boundary recognized in Hole 1138A is not unexpected considering the strong glacial event (Mi-1) postulated for this time interval (Zachos et al., 2001). A hiatus spanning this time interval is recognized at several Southern Ocean sites (Wright and Miller, 1993).

FUTURE REFINEMENTS IN THE DIATOM BIOZONATION

The agreement between middle and late Miocene diatom ages and ^{40}Ar-^{39}Ar ages reinforces the reliability of several diatom datums in this interval. As discussed by Ramsay and Baldauf (1999), many Neogene diatom datums still require precise calibration to the polarity timescale or strontium isotope stratigraphy, and calibration in multiple drill cores is necessary in order to ascertain the synchroneity of datums between different regions of the Southern Ocean. It appears, however, that most Miocene diatom bioevents at Kerguelen Plateau sites do not display the degree of diachronism interpreted by Ramsay and Baldauf (1999). Censarek and Gersonde (2002) reach a similar conclusion for sites in the Atlantic sector of the Southern Ocean, further reinforcing the synchroneity of Miocene datums and general utility of diatom biostratigraphy in Miocene sequences from the Southern Ocean.

In the present study, a calibration of the LO of *N. denticuloides* is determined at Site 1138 through ^{40}Ar-^{39}Ar dating of a tephra layer in Core 183-1138A-19R. The LO of *N. denticuloides* occurs between 171.70 and 170.20 mbsf, and a mean age of 11.45 ± 0.22 Ma is derived from the tephra horizon at 170.81 mbsf (Fig. F7). In Hole 747A, the LO of *N. denticuloides* occurs between 61.47 and 59.97 mbsf (Harwood and Maruyama, 1992), in association with the Subchron C5An.1n/C5r.3r reversal at 61.30 mbsf (Fig. F7). The age calibration for this reversal is 11.94 Ma (Berggren et al., 1995), and the LO of *N. denticuloides* is assigned a calibrated age of ~11.7 Ma, due to the sample spacing uncer-

tainty. Therefore, the age calibration in Hole 747A of ~11.7 Ma is in close agreement to that of ~11.5 Ma determined in Hole 1138A.

A middle Miocene tephra horizon that occurs in association with the LO of *N. denticuloides* is also present in Hole 747A at 60.90 mbsf (Fig. F7). The middle Miocene tephra layer at Site 747 is more trachytic in composition (Morche et al., 1992) than the Site 1138 ash, but it is possible that the two horizons represent the same eruptive event. The LO of *N. denticuloides* falls immediately below the tephra horizons in both drill cores (Fig. F7), although there is some uncertainty in the placement of the datum levels because of sample spacing gaps. In spite of this uncertainty, the tephra horizons are correlative within the limits of current age control for the two drill cores (Fig. F7). A middle Miocene tephra layer was also reported at Site 737 (Northern Kerguelen Plateau) in Section 119-737B-5R-1 (Morche et al., 1991). This tephra, however, falls well above the LO of *Denticulopsis dimorpha* (Baldauf and Barron, 1991) and is therefore late Miocene in age and not correlative with the ash horizons at Sites 747 and 1138.

The LO of *N. denticuloides* is well documented from drill cores on Maud Rise (Leg 113) and Meteor Rise (Leg 177) (Gersonde and Burckle, 1990; Censarek and Gersonde, 2002). In the Maud Rise sections, Censarek and Gersonde (2002) recalibrated the LO of *N. denticuloides* to the Berggren et al. (1995) timescale. An age of 11.82 Ma is calculated for this datum in Hole 689B, and an age of 11.78 Ma is calculated in Hole 690B. A similar age of 11.86 Ma is also determined at Site 1092, which is located at a more northerly position within the modern PFZ (Censarek and Gersonde, 2002). These ages are in general agreement with those derived from Kerguelen Plateau sections.

The upper Pliocene–Pleistocene diatom zonation for the Southern Ocean is presently defined by datums that are widely separated in time. If the LO of *Fragilariopsis barronii* is not utilized in the zonal scheme (due to taxonomic difficulties in separating from *F. barronii* from *F. kerguelensis*), a large gap is present between the LO of *Thalassiosira kolbei* (1.9 Ma) and the LCO of *Actinocyclus ingens* (0.66–0.70 Ma). Future detailed studies on the Kerguelen Plateau will hopefully identify other datums within this interval, such as the first abundant occurrence datum of *Thalassiosira elliptipora* (~1.1 Ma) utilized by Zielinski and Gersonde (2002). Distinct Pleistocene acmes of *Actinocyclus ingens* were not identified in Hole 1138A, which would have allowed application of ages derived from northern Southern Ocean sites (Gersonde and Bárcena, 1998). Also, Pleistocene samples from Hole 1138A contained only rare specimens of *Fragilariopsis matuyamae*, a taxon that has been shown to be biostratigraphically useful at northern Antarctic and Subantarctic sites (Gersonde and Bárcena, 1998; McMinn et al., 2001). An uppermost Pleistocene acme of *Hemidiscus karstenii,* however, did allow application of the Southern Ocean LO datum (0.21 Ma) for this taxon.

Several diatom events recognized in Hole 1138A are identified as potentially useful datums for future studies on the Kerguelen Plateau and application in a revised Neogene diatom zonation. Useful markers in the upper Miocene include the FO of *Hemidiscus karstenii* f. 1 (of Ciesielski, 1983), the LO of *Denticulopsis crassa,* and the FO and LO of *Hemidiscus triangularus.* The FO of *H. triangularus,* for example, has already been applied in revised zonal schemes for the Atlantic sector of the Southern Ocean (Censarek and Gersonde, 2002). Additionally, the FO of *Thalassiosira lentiginosa* var. *ovalis* and the FO and LO of *Fragilariopsis heardensis* are potentially useful in the upper Pliocene, and the LO of *Rouxia antarctica* may be of use in the Pleistocene.

S.M. Bohaty et al.
Neogene Diatom and Tephra Stratigraphy

14

PALEOENVIRONMENTAL CONSIDERATIONS

Only limited paleoenvironmental information can be inferred from the qualitative diatom abundance data collected in the present study. The diatom assemblages recovered in Hole 1138A are predominantly planktonic in composition. Benthic taxa, such as *Cocconeis* spp. and *Rhabdonema* spp., were observed in low abundance (≤1% of the assemblage) throughout the section (Table T1). These specimens are interpreted to have been laterally transported from shallower areas, possibly by the mechanism of turbidity currents described by Coffin, Frey, Wallace, et al. (2000).

The lower to middle Pliocene sediments of Hole 1138A are rich in biosiliceous material and contain numerous diatom taxa with a modern Subantarctic distribution or a known fossil distribution restricted primarily to the middle latitudes. These taxa include *Hemidiscus karstenii, N. reinholdii, Proboscia* spp., and, possibly, *Azpeitia harwoodii*. Similar preservation of lower Pliocene biosiliceous material has been described in many Southern Ocean sections. This observation, in addition to the presence of numerous "warm-water" diatom, radiolarian, and silicoflagellate taxa, has been interpreted as a reflection of early Pliocene surface water warming in the Southern Ocean (e.g., Abelmann et al., 1990; Bohaty and Harwood, 1998). Quantitative documentation of these assemblages on the Kerguelen Plateau is necessary to delineate early to late Pliocene warming and cooling events and related shifts in the position of the PFZ.

Numerous samples from the Pliocene–Pleistocene interval of Hole 1138A contain moderately abundant nannofossil (Fig. F2) and foraminiferal assemblages. Nannofossil assemblages for this time interval are not well documented on the Kerguelen Plateau. Nannofossil abundance and assemblage composition may similarly provide useful paleoenvironmental information regarding shifts in the PFZ. Additionally, alkenones may be present in the nannofossil-bearing intervals and may provide independent estimates of high-latitude surface temperatures during the Pliocene and Pleistocene.

Fragilariopsis curta is a modern diatom taxon that is ecologically associated with sea-ice environments. In Pleistocene–Holocene sediment studies, the quantitative abundance of *F. curta* is used as a proxy for the relative influence of sea ice (Gersonde and Zielinski, 2000). In Hole 1138A, the FO of *F. curta* is recorded in the upper Pliocene at 74.04 mbsf. This first occurrence of *F. curta* at ~3.0 Ma on the Central Kerguelen Plateau most likely represents a late Pliocene expansion of sea-ice influence and cooling. Several modern taxa, such as *Asteromphalus parvulus* and *Fragilariopsis separanda,* also have first occurrences in the upper Pliocene and lower Pleistocene in Hole 1138A. These first occurrences, combined with the progressive extinction of several taxa through this interval, represent the initial development of the modern endemic diatom flora in the Southern Ocean. Progressive endemism in Antarctic diatom assemblages has also been associated with regional late Pliocene–early Pleistocene cooling (e.g., Harwood, 1991).

SUMMARY

Although rotary drilled, the Neogene section in Hole 1138A provides insight into the geologic and paleoceanographic history of the Central Kerguelen Plateau. A moderately well constrained Neogene age-depth

S.M. Bohaty et al.
NEOGENE DIATOM AND TEPHRA STRATIGRAPHY

15

model for the hole is derived from 36 diatom datums and 5 nannofossil and planktonic formanifer datums, as well as magnetostratigraphic constraint. Four "outlying" planktonic foraminifer and nannofossil datums are inconsistent with the age model defined by the other datums. Five ^{40}Ar-^{39}Ar ages from tephra horizons provide further age constraint and are in good agreement with the biostratigraphic age interpretations. Previous paleomagnetic calibrations of the LO of *N. denticuloides* are directly confirmed in Hole 1138A by a ^{40}Ar-^{39}Ar age determination of 11.45 ± 0.22 Ma for a tephra horizon overlying this datum.

An important feature of the Neogene strata recovered at Site 1138 is the presence of dispersed tephra and several discrete tephra horizons. Ash material at this site is interpreted to have originated from Heard Island and deposited from both primary ash fall and distal turbidity plumes (Coffin, Frey, Wallace, et al., 2000). Neogene tephras at Site 1138 are predominantly trachytic to rhyolitic in composition and document the nature of late Cenozoic evolution of Kerguelen volcanism. Within the resolution of the age information presented here, the middle Miocene tephra layers documented at Sites 747 and 1138A are correlative.

Hole 1138A contains an expanded lower Pliocene–upper Pleistocene section (~105 m) relative to most other drill cores recovered on the Kerguelen Plateau. In comparison, only ~29 m of Pliocene–Pleistocene section was recovered in nearby Hole 747A. In addition to high sedimentation rates, the preservation of both carbonate and siliceous microfossils is a distinctive feature of upper Miocene to Pleistocene sediments in Hole 1138A. Furthermore, a detailed investigation of late Neogene shifts in the PFZ is possible at this site through future piston coring operations.

SYSTEMATIC PALEONTOLOGY

A full systematic treatment with synonymies for all diatom taxa identified in the present study is not given here. Individual species are annotated with the original author name and short references to accessible and quality illustrations. A few brief notes are also given on unusual varieties, problematic taxa, and stratigraphic distributions. Several specimens are illustrated in Plates P1, P2, and P3. Our taxonomy is based primarily on descriptions and illustrations of taxa from Neogene sections in Antarctic and Subantarctic waters. The following reports form the basis of this pool of literature: Abbott (1974), McCollum (1975), Gombos (1977), Schrader (1976), Fenner et al. (1976), Akiba (1982), Ciesielski (1983, 1986), Gersonde and Burckle (1990), Gersonde (1991), Fenner (1991), Baldauf and Barron (1991), Harwood and Maruyama (1992), Mahood and Barron (1996a, 1996b), Gersonde and Bárcena (1998), Bohaty et al. (1998), Zielinski and Gersonde (2002), and Censarek and Gersonde (2002). Several reports from North Pacific cores and outcrops also provide taxonomic guidelines for Miocene diatom taxa, including Barron (1985a), Akiba (1986), Akiba and Yanagisawa (1986), Yanagisawa and Akiba (1990), Akiba et al. (1993), Yanagisawa (1995), Gladenkov and Barron (1995), and Komura (1998).

The goal of the current investigation is to identify important marker datums and delineate zonal boundaries. Some taxonomic problems, however, arose in the identification of several taxa. Along with the common problem of taxonomic variability within and between samples, the presence of intermediate or transitional forms complicated the

precise placement of datum levels. Intermediate forms, for example, were noted between *Thalassiosira jacksonii* and *T. inura, Fragilariopsis aurica* and *F. barronii, Fragilariopsis praeinterfrigidaria* and *F. interfrigidaria, F. interfrigidaria* and *F. weaveri,* and *F. barronii* and *F. kerguelensis.* In the *F. barronii* lineage, however, there is a transition over a narrow stratigraphic interval from intermediate *F. aurica–F. barronii* forms to *F. barronii.* Stricter taxonomic divisions than those currently defined are needed to further refine the Southern Ocean zonal scheme. Ideally, the zonal boundaries are those defined by the first or last common appearance of "sensu stricto" forms.

A number of Neogene diatom taxa have recently been transferred from the genus *Nitzschia* to *Fragilariopsis* (Gersonde and Bárcena, 1998; Zielinski and Gersonde, 2002; Censarek and Gersonde, 2002). We have followed these revisions, with a few exceptions. *Nitzschia miocenia* and *N. reinholdii,* for example, are currently left assigned to *Nitzschia*, pending further SEM investigation of these taxa.

Actinocyclus actinochilus (Ehrenberg) Simonsen, 1982, pp. 101–116, pl. 1–4; Villareal and Fryxell, 1983, p. 461, figs. 21–32.

Actinocyclus curvatulus Janisch in Schmidt; Koizumi, 1973, p. 831, pl. 1, figs. 1–6; Akiba, 1982, pp. 41, 42, pl. 5, figs. 5a–6.

Actinocyclus dimorphus (Castracane) Harwood and Maruyama, 1992, p. 700, pl. 12, fig. 16(?); pl. 13, figs. 3–5; pl. 17, figs. 19, 20 (Pl. P1, fig. 11).

Actinocyclus fasciculatus Harwood and Maruyama, 1992, p. 700, pl. 13, figs. 14, 15; Censarek and Gersonde, 2002, p. 350, pl. 1, fig. 5.

Actinocyclus ingens Rattray; Akiba, 1982, p. 42, pl. 5, figs. 7–14; Gersonde, 1990, pp. 791, 792, pl. 1, figs. 1, 3–5; pl. 3, figs. 8, 9; pl. 4, fig. 1.

Actinocyclus ingens var. *nodus* Baldauf in Baldauf and Barron, 1980, p. 104, pl. 1, figs. 5–9; Gersonde, 1990, p. 792, pl. 1, fig. 6; pl. 3, figs. 4–7; Censarek and Gersonde, 2002, p. 350, pl. 1, fig. 4.

Actinocyclus ingens var. *ovalis* Gersonde, 1990, p. 792, pl. 1, fig. 7; pl. 3, figs. 1–3; pl. 5, figs. 4, 7; pl. 6, figs. 1, 4–5; Censarek and Gersonde, 2002, p. 350, pl. 1, figs. 6, 8 (Pl. P1, figs. 2, 3).
Remarks: Harwood and Maruyama (1992) transferred *A. ingens* var. *ovalis* to the genus *Hemidiscus* and elevated the variety *"ovalis"* to species status. We retain the original designation, however, because of its close affinity with *A. ingens.* In addition, *Hemidiscus ovalis* Lohman (1938, pp. 91, 92, pl. 22, fig. 9) maintains priority over *H. ovalis* Harwood and Maruyama (1992). Specimens identified in the present study as *A. ingens* var. *ovalis* are restricted to morphologies with a strongly oval to broadly rounded lanceolate valve outline (see Pl. P1, figs. 2, 3). *A. ingens* var. *ovalis* is oval shaped and symmetrical in valve outline and possesses reduced areolation in the central area; these features distinguish it from *Hemidiscus karstenii.*

Actinocyclus ingens var. 1 (Pl. P1, figs. 7, 12).
Description and remarks: This precursor form to *A. ingens* is characterized by closely packed areolae and light silicification of the central area. In Hole 1138A, *A. ingens* var. 1 has a lowest occurrence in Sample 183-1138A-23R-CC (210.85 mbsf), just below the FO of *A. ingens* s.s.

Actinocyclus ingens var. 2 (Pl. P1, figs. 8, 9).
Description and remarks: *A. ingens* var. 2 is a distinctive form of *A. ingens* with a small valve diameter (≤25 μm) and a hyaline central area. It is distinguished from *A. ingens* var. A of Harwood and Maruyama (1992, p. 700, pl. 12, figs. 4, 5) by its small valve diameter. This form was only observed in Pleistocene Sample 183-1138A-4R-1, 25–26 cm, and, therefore, may have a restricted range.

Actinocyclus karstenii Van Heurck; Harwood and Maruyama, 1992, p. 700, pl. 13, figs. 1, 2, 6–8, 10, 11, 13; Mahood and Barron, 1996b, p. 288, pl. 3, fig. 5; Zielinski and Gersonde, 2002, p. 253, pl. 3, figs. 4, 5, 7–9, 12(?).

Actinocyclus maccollumii Harwood and Maruyama, 1992, p. 700, pl. 17, fig. 29.

Actinoptychus senarius (Ehrenberg) Ehrenberg; Akiba, 1986, pl. 29, fig. 2.

Araniscus lewisianus (Greville) Komura, 1998, pp. 6–8, figs. 20–22, 87–104, and text fig. 1.
Basionym: *Coscinodiscus lewisianus* Greville; Schrader, 1973, p. 703, pl. 8, figs. 1–6, 10, 15; Schrader, 1976, p. 631, pl. 14, fig. 3; Harwood and Maruyama, 1992, p. 702, pl. 6, fig. 13.

Asterolampra tela Gombos and Ciesielski, 1983, p. 600 as *Asterolampra* sp. A, but in pl. 3, figs. 1–4 as *Asterolampra tela.*

Asteromphalus hookeri Ehrenberg; Akiba, 1982, p. 42, pl. 1, fig. 1; Bohaty et al., 1998, pl. 2, fig. 5.

Asteromphalus kennettii Gersonde, 1990, p. 793, pl. 2, fig. 1; pl. 6, fig. 2; Harwood and Maruyama, 1992, p. 701, pl. 11, fig. 3; Censarek and Gersonde, 2002, p. 350, pl. 1, fig. 2.

Asteromphalus oligocenicus Schrader and Fenner, 1976, pp. 965, 966, pl. 21, figs. 8, 13, 14; pl. 28, fig. 1.

Asteromphalus parvulus Karsten; Fenner et al., 1976; p. 769, pl. 4, figs. 20, 21.
Note: *A. parvulus* and *A. hookeri* were grouped together in the present study (Table T1).

Asteromphalus symmetricus Schrader and Fenner, 1976, p. 966, pl. 21, figs. 7, 10–12.

Azpeitia gombosi Harwood and Maruyama, 1992, p. 701, pl. 3, figs. 1, 2.

Azpeitia harwoodii Bohaty and Shiono n. sp. (Pl. P1, fig. 10; Pl. P3, figs. 1–6, 10–13).
Synonym: *Azpeitia* sp. B of Shiono, 2000a (doctoral thesis), pl. 34, figs. 1–6; pl. 35, figs. 1–6.
Description: Valve is heavily silicified and circular in outline. Valve diameter ranges from 18 to 60 µm. Valve face is flat with no central depression. Areolae are roughly equal in size across valve face, with four to six areolae in 10 µm. The arrangement of the areolae on the valve face varies from to sublineate to subeccentric, and the packing of areolae in the central area ranges from very dense to moderately dense. The valve possesses a steep mantle with an areolate margin. A thin mantle ridge is present between the valve face and mantle on some specimens, but this feature is commonly absent. Two to three areolae are present on the mantle between the valve face and valve edge. A central labiate process is positioned slightly off center, with a small, round external opening that lacks an external tube structure. Six to ten marginal, equally spaced labiate processes are also present with small, round external openings near the valve face–mantle transition. Both central and marginal labiate processes open internally to a flared tube structure. Some specimens display a weakly developed central hyaline ring on the exterior of the valve and/or increased silicification between the central areolae.
Type Level and Locality: Sample 183-1138A-11R-6, 100–101 cm, ODP Hole 1138A, Central Kerguelen Plateau.
Holotype: Pl. P3, fig. 1 (high and low focus).
Type Specimen: Slide deposited in the California Academy of Science microfossil slide collection, CAS Slide Number 221034, CAS Accession Number 619994. Specimen is mounted in Norland optical adhesive and marked with a double scribe circle on cover slip.
Stratigraphic Distribution: *A. harwoodii* is documented in Pliocene sections from both the Southern Ocean and North Pacific. In the present study, *A. harwoodii* was observed in lower Pliocene sediments of ODP Hole 1138A, where it is

common in all examined samples from Core 183-1138A-11R. The stratigraphic range for *A. harwoodii* in Hole 1138A (corresponding to Core 183-1138A-11R), falls within Subchron C2Ar, with an estimated age range of ~4.2 to 3.7 Ma. In the Hole 1138A section, however, the FO of *A. harwoodii* lies just above an unconformity and its lower range may therefore be truncated. *A. harwoodii* has also been observed in lower Pliocene samples from ODP Hole 1165B (Bohaty and Whitehead, unpubl. data), located on the Antarctic continental rise (to the south of Site 1138).

In the northwest Pacific, *A. harwoodii* is recorded in Pliocene samples from DSDP Hole 579A. In this section, rare specimens of *A. harwoodii* were observed in middle Pliocene Samples 86-579A-11-2, 30–31 cm, and 11-5, 30–31 cm, and in lower Pleistocene Samples 4-3, 12–13 cm, and 5-5, 25–26 cm. The Pliocene interval of Hole 579A is assigned an age of ~3.6 to 3.4 Ma, which is a slightly younger occurrence than documented at Southern Ocean Site 1138. The Pleistocene occurrence of *A. harwoodii* in Hole 579A may be due to reworking, based on the rarity of specimens.

Remarks: A pseudonodulus on the valve margin of *A. harwoodii* was not identified in SEM examination of specimens from Hole 1138A. A pseudonodulus, however, was noted on some specimens from Hole 579A (Shino, 2000b, pl. 34, fig. 4). Pending further SEM work on this taxon, we have elected not to include the presence of a pseudonodulus as part of the description of *A. harwoodii.*

A. harwoodii belongs to the "*Azpeitia nodulifera* group" described by Shiono and Koizumi (2002). Taxa within this group are characterized by the absence of a marginal hyaline area. *A. harwoodii* is taxonomically similar to *Azpeitia nodulifera* (see Fryxell et al., 1986, p. 19, 20, figs. XVII, XVIII-1, 2, 4, 5, and XXX-3, 4), a modern species found in warm-water regions (Hasle and Syvertsen, 1996). *A. harwoodii,* however, is typically smaller in diameter (18–55 µm) than *A. nodulifera* (20–100 µm). Additionally, *A. harwoodii* is more heavily silicified than *A. nodulifera* and lacks a well-developed mantle ridge.

A form similar to *A. harwoodii* was described by Shiono and Koizumi (2002) as "*Azpeitia* sp. A." In contrast to *A. harwoodii, Azpeitia* sp. A is characterized by a slight central depression and radial arrangement of valve-face areolae.

Paleoecology: Given the warm-water affinity of modern taxa in the "*Azpeitia nodulifera* group" (Hasle and Syvertsen, 1996; Shiono and Koizumi, 2002), the presence of *A. harwoodii* at Sites 579, 1138, and 1165 may be associated with local Pliocene warming at these sites in the North Pacific and Southern Oceans.

Derivation of Name: This species is named in honor of Dr. David Harwood at the University of Nebraska-Lincoln for his contributions to the development of Southern Ocean diatom biostratigraphy.

Authorship: The description of this new taxon is co-authored by Dr. Masamichi Shiono at Hokkaido University, Sapporo, Japan.

Azpeitia tabularis (Grunow) Fryxell and Sims in Fryxell et al., 1986, pp. 16–18, figs. XIV, XV, XXX-I; Censarek and Gersonde, 2002, p. 350, pl. 1, fig. 7.

Bogorovia gombosii (Desikachary) Yanagisawa, 1995, pp. 27–29, figs. 4-1, 4-2, 5-1, 5-2.

Bogorovia veniamini Jousé ex Yanagisawa, 1995, pp. 29–31, figs. 4-3 through 4-10, 8-1 through 8-10.

Cavitatus jouseanus (Sheshukova) Williams; Akiba et al., 1993, pp. 20–22, figs. 6-19, 6-20; Censarek and Gersonde, 2002, p. 350, pl. 5, fig. 12.

Cavitatus miocenicus (Schrader) Akiba and Yanagisawa in Akiba et al., 1993, p. 28, figs. 9-1 through 9-11.

Cavitatus rectus Akiba and Hiramatsu in Akiba et al., 1993, pp. 28–30, figs. 6-7 through 6-15.

Cestodiscus pulchellus Greville; Harwood and Maruyama, 1992, p. 701, pl. 3, figs. 6, 7.

Chaetoceros bulbosum (Ehrenberg) Heiden; Akiba, 1982, p. 42, pl. 7, fig. 9; Bohaty et al., 1998, pl. 5, fig. 12.

Chaetoceros lorenzianus Grunow; Harwood et al., 2000, fig. 7-q.

Chaetoceros sp. A of Harwood and Maruyama, 1992, p. 701, pl. 19, figs. 5–7.

Corethron criophilum Castracane; Krebs, 1983, p. 285, pl. 2, fig. 4a, b; Harwood and Maruyama, 1992, p. 701, pl. 19, figs. 8–11; pl. 5, fig. 15.

"Coscinodiscus" rhombicus Castracane; Barron, 1985b, p. 782, figs. 9.11, 9.12; Ciesielski, 1986, pl. 5, fig. 12; Harwood and Maruyama, 1992, p. 702, pl. 3, figs. 16, 17; pl. 8, figs. 12, 13; pl. 11, fig. 1; Censarek and Gersonde, 2002, p. 350, pl. 1, fig. 3.
Remarks: This taxon may be better placed in the genus *Araniscus* Komura 1998.

Coscinodiscus marginatus Ehrenberg; Schrader, 1973, p. 703, pl. 20, figs. 7, 10, 12, 13; Schrader, 1976, p. 631, pl. 12, fig. 2.

Crucidenticula ikebei Akiba and Yanagisawa, 1986, pp. 485, 486, pl. 1, figs. 1, 2; Yanagisawa and Akiba, 1990, pp. 228, 229, pl. 1, figs. 10–12; pl. 8, figs. 8–13.
Remarks: Specimens identified here as *C. ikebei* in Hole 1138A are similar to forms illustrated as *Crucidenticula kanayae* by Harwood and Maruyama (1992, pl. 7, fig. 15). The specimens identified in Hole 1138A are grouped as *C. ikebei,* rather than *Crucidenticula sawamurae,* because they possess slightly tapered apices.

Crucidenticula nicobarica Akiba and Yanagisawa, 1986, pp. 486, 487, pl. 1, fig. 9; pl. 2, figs. 1–7; pl. 5, figs. 1–9; Yanagisawa and Akiba, 1990, p. 232, pl. 1, figs. 23–29; Censarek and Gersonde, 2002, p. 351, pl. 2, figs. 25, 26.

Dactyliosolen antarcticus Castracane; Hasle, 1975, pp. 119–121, figs. 90–100, 109–112; Harwood and Maruyama, 1992, p. 702, pl. 18, fig. 12.
Comments: Only the wedge-shaped, girdle-band ends of *D. antarcticus* are commonly found in sediment samples.

"Denticula" sp. cf. *Denticula norwegica* Schrader in Schrader and Fenner, 1976, p. 978, pl. 1, fig. 38; Akiba and Yanagisawa, 1986, p. 487, pl. 2, figs. 15–21; pl. 6, figs. 1–9.

Denticulopsis crassa Yanagisawa and Akiba, 1990, pp. 248, 249, pl. 3, figs. 21–27; pl. 12, figs. 1–8; Censarek and Gersonde, 2002, p. 351, pl. 2, fig. 12.

Denticulopsis dimorpha var. *areolata* Yanagisawa and Akiba, 1990, p. 257, pl. 4, figs. 40, 41, 50–54; pl. 5, figs. 13–17; pl. 6, figs. 1–5, 15–23; pl. 12, figs. 15, 16.

Denticulopsis dimorpha Schrader (Simonsen) var. *dimorpha* Yanagisawa and Akiba, 1990, pp. 254, 255, pl. 4, figs. 42–49; pl. 7, figs. 14–16.

Denticulopsis "hustedtii var. *aspera"* Maruyama in Harwood and Maruyama, 1992, p. 702, pl. 10, figs. 8–11, 15, 16.
Remarks: Because of taxonomic revisions in the *Denticulopsis* group by Yanagisawa and Akiba (1990), this form should be renamed, or the variety name *"aspera"* should be elevated to species status.

Denticulopsis hyalina (Schrader) Simonsen; Yanagisawa and Akiba, 1990, pp. 240, 241, pl. 2, figs. 14, 33, 34; pl. 9, figs. 8, 9.

Denticulopsis maccollumii Simonsen; Yanagisawa and Akiba, 1990, pp. 264, 265, pl. 2, figs. 39–41; Harwood and Maruyama, 1992, p. 702, pl. 6, fig. 22; pl. 7, fig. 17; pl. 9, fig. 27; Censarek and Gersonde, 2002, p. 351, pl. 2, figs. 32–34.

Denticulopsis ovata (Schrader) Yanagisawa and Akiba, 1990, pp. 257, 258, pl. 6, figs. 6–14, 24–32; Censarek and Gersonde, 2002, p. 351, pl. 2, figs. 13–20.
Synonym: *Denticulopsis meridionalis* Harwood and Maruyama, 1992, pp. 702, 703, pl. 6, figs. 1–4; pl. 7, figs. 1–4, 6–9, 11–13; pl. 9, figs. 1–4, 10–14; pl. 10, fig. 7.

Denticulopsis praedimorpha Barron ex Akiba var. *praedimorpha* Yanagisawa and
    Akiba, 1990, pp. 251, 252, pl. 4, figs. 3–5, 10, 12–17, 39; pl. 5, figs. 4–12; Cen-
    sarek and Gersonde, 2002, p. 351, pl. 2, figs. 1–7.

Denticulopsis simonsenii Yanagisawa and Akiba, 1990, pp. 242, 243, pl. 3, figs. 1–
    3; pl. 11, figs. 1, 5; Censarek and Gersonde, 2002, p. 351, pl. 2, figs. 21–24.
    Remarks: *D. simonsenii* was separated from *Denticulopsis vulgaris* following
the taxonomy of Yanagisawa and Akiba (1990). *D. vulgaris* is characterized by re-
duced punctation on the valve face, with striae positioned near each pseudosep-
tum, whereas *D. simonsenii* is characterized by full punctation between the
psuedospeta. However, some intermediate forms were observed, and poorly pre-
served specimens in some intervals were difficult place into either group.

Denticulopsis vulgaris (Okuno) Yanagisawa and Akiba, 1990, pp. 243, 244, pl. 3,
    figs. 4–8; pl. 11, figs. 2, 6–10.
    Remarks: See notes under *Denticulopsis simonsenii.*

Entopyla spp. (Pl. P2, fig. 19).
    Remarks: A distinctive specimen belonging to the genus *Entopyla* was noted
in Sample 183-1138A-8R-5, 100–101 cm (see Pl. P2, fig. 19).

Eucampia antarctica (Castracane) Mangin; Krebs, 1983, p. 285, pl. 3, figs. 3a, b;
    Mahood and Barron, 1996b, p. 290, pl. 1, figs. 1–3; pl. 7, figs. 1, 2.

Eucampia antarctica var. *"twista"*
    Remarks: This variety of *E. antarctica* has not been formally described and is
characterized by rotation (up to 90°) on the valvar plane, similar to the Paleo-
gene species *Hemiaulus rectus* var. *twista* Fenner.

Fragilariopsis arcula (Gersonde) Gersonde and Bárcena, 1998, p. 92; Censarek
    and Gersonde, 2002, p. 351, pl. 3, figs. 15–18.
    Basionym: *Nitzschia arcula* Gersonde, 1991, pp. 143, 144, pl. 2, fig. 4; pl. 4,
fig. 4; pl. 5, figs. 1–6.

Fragilariopsis aurica (Gersonde) Gersonde and Bárcena, 1998, p. 92; Censarek
    and Gersonde, 2002, p. 351, pl. 3, figs. 9–12; Zielinski and Gersonde, 2002, p.
    257, pl. 1, figs. 13–15.
    Basionym: *Nitzschia aurica* Gersonde, 1991, pp. 144–146, pl. 1, figs. 18–25;
pl. 3, fig. 5; pl. 4, figs. 5, 6; pl. 7, fig. 6.

Fragilariopsis barronii (Gersonde) Gersonde and Bárcena, 1998, p. 92; Zielinski
    and Gersonde, 2002, p. 257, pl. 1, figs. 29–31.
    Basionym: *Nitzschia barronii* Gersonde, 1991, pp. 146, 147, pl. 3, fig. 6; pl. 4,
figs. 1–3; pl. 5, figs. 7–17.
    Remarks: Intermediate forms between *F. barronii* and *F. aurica* were noted
near the FO of *F. barronii*. These intermediate forms were recorded separately as
Fragilariopsis sp. cf. *F. barronii.*

Fragilariopsis clementia (Gombos) Zielinski and Gersonde, 2002, p. 33; Censarek
    and Gersonde, 2002, p. 351, pl. 3, figs. 7, 8.
    Basionym: *Nitzschia clementia* Gombos, 1977, p. 595, pl. 8, figs. 18, 19; Ger-
sonde and Burckle, 1990, p. 779, pl. 2, figs. 22, 23 (Pl. P2, figs. 8, 9).

Fragilariopsis curta (Van Heurck) Hustedt; Hasle, 1965, pp. 32, 33, pl. 6, fig. 6; pl.
    12, figs. 2–5; pl. 13, figs. 1–6; pl. 16, fig. 6; pl. 17, fig. 5.
    Basionym: *Fragilaria curta* Van Heurck, 1909, p. 24, pl. 3, fig. 37.
    Synonym: *Nitzschia curta* (Van Heurck) Hasle, 1972, p. 115; Krebs, 1983, p.
286, pl. 4, fig. 4; Hasle and Medlin, 1990, p. 181, pl. 24.6, figs. 2–5.

Fragilariopsis cylindrus (Grunow) Krieger in Helmcke and Krieger; Hasle, 1965,
    pp. 34–37, pl. 12, figs. 6–12; pl. 14, figs. 1–10; pl. 17, figs. 2–4.
    Synonym: *Nitzschia cylindrus* (Grunow) Hasle, 1972, p. 115; Hasle and Med-
lin, 1990, p. 181, pl. 24.6, figs. 6–11.

Fragilariopsis donahuensis (Schrader) Censarek and Gersonde, 2002, p. 350, pl. 3,
    figs. 13, 14.

Basionym: *Nitzschia donahuensis* Schrader, 1976, p. 633, pl. 2, fig. 30; Gersonde and Burckle, 1990, p. 780, pl. 1, figs. 16–18.

Fragilariopsis efferans (Schrader) Censarek and Gersonde, 2002, p. 350.
Basionym: *Nitzschia efferans* Schrader, 1976, p. 633, pl. 2, figs. 1, 3, 5–7.

Fragilariopsis fossilis (Frenguelli) Medlin and Sims, 1993, pp. 332, 333; Censarek and Gersonde, 2002, p. 351, pl. 3, figs. 3, 4; Zielinski and Gersonde, 2002, p. 257, pl. 1, figs. 5, 6.
Synonym: *Nitzschia fossilis* (Frenguelli) Kanaya in Kanaya and Koizumi; Schrader, 1973, p. 707, pl. 4, figs. 9–11, 24, 25; Gersonde and Burckle, 1990, p. 780, pl. 1, figs. 19, 20.

Fragilariopsis heardensis Bohaty n. sp. (Pl. **P2,** figs. 1–7; Pl. **P3,** fig. 9).
Description: Valve is clavate in outline and heteropolar. Ends are broadly rounded in shape, with one inflated end and one narrow, tapered end. There are 9 to 14 transapical striae in 10 µm across the valve face. Striae are straight, except at the terminal margin of the inflated end, where they are curved. Valve is lightly silicified, and small areolae that form uniseriate striae are faintly visible in the light microscope when mounted in a high-index medium. The valve is 35 to 85 µm in length and 10 to 12 µm wide at its widest point. Raphe is positioned on the margin.
Comments: This form is morphologically similar to *Fragilariopsis clementia* (see Gombos, 1977, pl. 8, figs. 18, 19; Gersonde and Burckle, 1990, pl. 2, figs. 22, 23) and *Fragilariopsis lacrima* (see Gersonde, 1991, pl. 1, figs. 1–6, 26; pl. 2, figs. 1–3). *F. heardensis,* however, is characterized by a more inflated, claviform shape than these two taxa. Additionally, *N. clementia* possesses more prominent costae when viewed in the light microscope and *F. lacrima* possesses coarser areolation. *F. heardensis, F. clementia,* and *F. lacrima* are compared in Plate **P2;** illustrated specimens of *F. lacrima* possess finer areolation than is typical of the taxon (Pl. **P2,** figs. 10, 11). Other taxa, such as *Nitzschia efferens* Schrader and *Nitzschia claviceps* Schrader show similarities to *F. heardensis* but also are coarser in their areolar structure. *F. heardensis* is also separated stratigraphically from these older Miocene taxa.
A range of *F. heardensis* morphologies was recognized in Hole 1138A, with differences in the coarseness of transapical striae, valve length, and the shape of the valve ends (highly rounded to broadly rounded). We have attempted to illustrate variation within this group, and the "end-members" are best represented by figures 1 and 3 on Plate **P2.**
Type Level and Locality: Sample 183-1138A-8R-5, 100–101 cm, ODP Hole 1138A, Central Kerguelen Plateau.
Holotype: Pl. **P2,** fig. 1a (differential interference contrast) and Pl. **P2,** fig. 1b (phase contrast).
Type Specimen: Slide deposited in the California Academy of Science microfossil slide collection, CAS Slide Number 221033, CAS Accession Number 619993. Specimen is mounted in Naphrax and is marked with a scribe circle on the coverslip.
Stratigraphic Distribution: *F. heardensis* was observed over a narrow stratigraphic interval (74.04–69.80 mbsf) in the upper Pliocene of Hole 1138A (Table **T1**). It is commonly fragmented as a result of its lightly silicified valve construction and is rare in all samples examined from Hole 1138A. *F. heardensis* was also observed in the upper Pliocene section of Hole 745B (S. Bohaty, unpubl. data), located on the Southern Kerguelen Plateau. Although also rare in Hole 745B, this taxon was noted in Samples 119-745B-13H-2, 10 cm; 13H-2, 42 cm; and 13H-3, 68 cm (111.10–113.18 mbsf). All three of these samples contain *Thalassiosira insigna* and *Thalassiosira vulnifica,* placing its range in a narrow interval within the *T. insigna–T. vulnifica* Zone in both Holes 745B and 1138A.
Derivation of Name: This taxon is named in reference to Heard Island, located 180 km northwest of Site 1138.

Fragilariopsis interfrigidaria (McCollum) Gersonde and Bárcena, 1998, p. 92; Zielinski and Gersonde, 2002, p. 259, pl. 1, figs. 20, 21.

S.M. Bohaty et al.
Neogene Diatom and Tephra Stratigraphy

22

Basionym: *Nitzschia interfrigidaria* McCollum, 1975, p. 535, pl. 9, figs. 7–9; Ciesielski, 1983, p. 655, pl. 1, figs. 11–18; Gersonde and Burckle, 1990, p. 780, pl. 1, figs. 1–3 (Pl. P2, figs. 15–18).

Remarks: Large forms of *F. interfrigidaria* (see Pl. P2, figs. 17, 18) were noted above the LO of *Fragilariopsis weaveri* within the *Thalassiosira insigna–Thalassiosira vulnifica* and *Thalassiosira vulnifica* Zones (71.30–66.80 mbsf). Although these specimens are included here as *F. interfrigidaria,* they may be taxonomically distinct from lower to middle Pliocene forms (see Pl. P2, figs. 15, 16). See also notes under *Fragilariopsis praeinterfrigidaria.*

Fragilariopsis januaria (Schrader) Bohaty n. comb.
Basionym: *Nitzschia januaria* Schrader, 1976, p. 634, pl. 2, figs. 25–29.
Remarks: Following the taxonomic revisions of Gersonde and Bárcena (1998), Zielinski and Gersonde (2002), and Censarek and Gersonde (2002), this taxon is transferred to the genus *Fragilariopsis.*

Fragilariopsis kerguelensis (O'Meara) Hustedt; Hasle, 1965, pp. 14–18, pl. 3, figs. 4, 5; pl. 4, figs. 11–18; pl. 5, figs. 1–11; pl. 6, figs. 2–4; pl. 7, fig. 9; pl. 8, fig. 10; pl. 16, figs. 3–5.
Synonym: *Nitzschia kerguelensis* (O'Meara) Hasle, 1972, p. 115; Fenner et al., 1976, p. 776, pl. 2, figs. 19–30; Hasle and Medlin, 1990, p. 181, pl. 24.2, figs. 11–18 (Pl. P2, fig. 13).
Remarks: *F. barronii* grades into *F. kerguelensis* in the upper part of its range (see illustrations of transitional forms in Zielinski and Gersonde, 2002, pl. 1, figs. 25–28). Identification of these two taxa is uncertain in the uppermost Pliocene–lower Pleistocene interval of Hole 1138A. Also, "early" forms of *F. kerguelensis* (see Pl. P2, fig. 13) possess smaller areolae than typical modern forms of *F. kerguelensis.*

Fragilariopsis lacrima (Gersonde) Gersonde and Bárcena, 1998, p. 92; Censarek and Gersonde, 2002, p. 351, pl. 3, figs. 5, 6; Zielinski and Gersonde, 2002, p. 259, pl. 1, figs. 8, 9.
Basionym: *Nitzschia lacrima* Gersonde, 1991, p. 148, pl. 1, figs. 1–6, 26; pl. 2, figs. 1–3 (Pl. P2, figs. 10, 11).

Fragilariopsis matuyamae Gersonde and Bárcena, 1998, p. 93, pl. 1, figs. 1–9, 13–16; pl. 2, figs. 1, 4, 5, 7–9; Zielinski and Gersonde, 2002, p. 259, pl. 1, figs. 10, 11.

Fragilariopsis obliquecostata (Van Heurck) Heiden in Heiden and Kolbe; Hasle, 1965, pp. 18–20, pl. 7, figs. 2–7.
Synonym: *Nitzschia obliquecostata* (Van Heurck) Hasle, 1972, p. 115; Fenner et al., 1976, pp. 776, 777, pl. 2, figs. 15–18.

Fragilariopsis praecurta (Gersonde) Gersonde and Bárcena, 1998, p. 92; Censarek and Gersonde, 2002, pp. 351, 352, pl. 3, figs. 19–21.
Basionym: *Nitzschia praecurta* Gersonde, 1991, pp. 148, 149, pl. 1, figs. 7–17; pl. 2, figs. 5, 6; pl. 3, figs. 3, 4; pl. 10, fig. 7.

Fragilariopsis praeinterfrigidaria (McCollum) Gersonde and Bárcena, 1998, p. 92; Zielinski and Gersonde, 2002, p. 259, pl. 1, figs. 22, 23; Censarek and Gersonde, 2002, p. 352, pl. 3, figs. 22, 23.
Basionym: *Nitzschia praeinterfrigidaria* McCollum, 1975, p. 535, pl. 10, fig. 1; Ciesielski, 1983, p. 655, pl. 2, figs. 1–8, 13–16; pl. 3, fig. 5.
Remarks: As noted above, intermediate forms between *F. praeinterfrigidaria* and *F. interfrigidaria* were noted in the Pliocene section of Hole 1138A. These forms possessed light silicification between the transapical costae.

Fragilariopsis pusilla (Schrader) Censarek and Gersonde, 2002, p. 350, pl. 3, fig. 25.
Basionym: *Nitzschia pusilla* Schrader, 1976, p. 634, pl. 2, fig. 20.

Fragilariopsis pseudonana (Hasle) Hasle; Hasle, 1965, pp. 22–24, pl. 1, figs. 7–14; pl. 4, figs. 20, 21; pl. 8, figs. 1–9; pl. 17, fig. 6.

S.M. Bohaty et al.
Neogene Diatom and Tephra Stratigraphy

23

Basionym: *Nitzschia pseudonana* Hasle, 1974, p. 427; Fenner et al., 1976, p. 777, pl. 2, figs. 6–11; Hasle and Medlin, 1990, p. 181, pl. 24.1, figs. 7–14.
Remarks: See Hasle and Syvertsen (1996) for comments on the taxonomy of this species.

Fragilariopsis rhombica (O'Meara) Hustedt; Hasle, 1965, pp. 24–26, pl. 1, fig. 6; pl. 4, fig. 19; pl. 6, fig. 5; pl. 8, fig. 11; pl. 9, figs. 1–6; pl. 10, figs. 2–6.
Synonym: *Nitzschia angulata* Hasle, 1972, p. 115; Fenner et al., 1976, p. 775, pl. 1, figs. 17–39; Hasle and Medlin, 1990, p. 181, pl. 24.1, fig. 6; pl. 24.2, fig. 19; pl. 24.4, figs. 1–6.

Fragilariopsis ritscheri Hustedt; Hasle, 1965, pp. 20, 21, pl. 1, fig. 20; pl. 3, fig. 3; pl. 4, figs. 1–10; pl. 5, figs. 12, 13; pl. 6, fig. 1; pl. 7, fig. 8.
Synonym: *Nitzschia ritscheri* (Hustedt) Hasle, 1972, p. 115; Fenner et al., 1976, p. 777, pl. 3, figs. 1–12; Hasle and Medlin, 1990, p. 181, pl. 24.1, fig. 20; pl. 24.2, figs. 1–10; pl. 24.3, fig. 9.

Fragilariopsis separanda Hustedt; Hasle, 1965, pp. 26, 27, pl. 9, figs. 7–10; pl. 10, fig. 1; Zielinski and Gersonde, 2002, p. 259, pl. 1, figs. 16, 17.
Synonym: *Nitzschia separanda* (Hustedt) Hasle, 1972, p. 115; Fenner et al., 1976, p. 777, pl. 1, figs. 1–16; Hasle and Medlin, 1990, p. 181, pl. 24.2, figs. 7–10.

Fragilariopsis weaveri (Ciesielski) Gersonde and Bárcena, 1998, p. 93; Zielinski and Gersonde, 2002, p. 260, pl. 1, figs. 18, 19.
Basionym: *Nitzschia weaveri* Ciesielski, 1983, p. 655, pl. 1, figs. 1–10.

Hemidiscus sp. cf. *H. cuneiformis* Wallich; Schrader, 1973, p. 706, pl. 24, fig. 14; Fenner et al., 1976, p. 774, pl. 11, fig. 17; Harwood and Maruyama, 1992, p. 703, pl. 11, fig. 11; Censarek and Gersonde, 2002, p. 352, pl. 4, fig. 5.

Hemidiscus karstenii Jousé; Abbott, 1974, p. 313, pl. 1, figs. D–F; Fenner, 1991, p. 108, pl. 1, fig. 2; Censarek and Gersonde, 2002, p. 352, pl. 3, fig. 27.

Hemidiscus karstenii f. 1 of Ciesielski, 1983, p. 656, pl. 4, figs. 2–5, but not pl. 4, fig. 1.
Remarks: This form is described with widely spaced areolae in the central area (Ciesielski, 1983). We strictly apply this definition and exclude specimens with closely packed areolae in the central area (Ciesielski, 1983, pl. 4, fig. 1). In contrast, Zielinski and Gersonde (2002, p. 260) apply "*H. karstenii* f. 1" to specimens with closely packed areolae in the central area.

Hemidiscus triangularus (Jousé) Harwood and Maruyama, 1992, p. 703; Censarek and Gersonde, 2002, p. 352, pl. 4, figs. 1–4.
Basionym: *Cosmiodiscus insignis* f. *triangula* Jousé; Ciesielski, 1983, p. 656, pl. 5, figs. 1–10; Ciesielski, 1986, p. 876, pl. 4, figs. 5, 6.

Hemiaulus incisus Hajós; Gombos and Ciesielski, 1983, pl. 20, fig. 6.

Hyalodiscus radiatus (O'Meara) Grunow in Cleve and Grunow; Harwood et al., 2000, p. 459, fig. 8g.

Ikebea sp. B of Scherer et al., 2000, p. 434, pl. 1, figs. 22, 23.

Lithodesmium minisculum Grunow in Van Heurck; Schrader, 1973, p. 706, pl. 12, figs. 7(?), 15, 17.

Navicula directa (Smith) Ralfs in Pritchard; Krebs, 1983, p. 285, pl. 3, fig. 7.

Neobrunia mirabilis (Brun in Brun and Tempère) Kuntze; Hendy, 1981, p. 11, pl. 1, figs. 1–3; pl. 2, figs. 4–7; pl. 3, figs. 10–13.
Synonym: *Brunia mirabilis* (Brun in Brun and Tempère) Tempère; Ciesielski, 1983, p. 655, pl. 7, figs. 1, 2.

Nitzschia denticuloides Schrader, 1976, p. 633, pl. 3, figs. 7, 8, 10, 12, 18–24; pl. 15, fig. 22; Harwood and Maruyama, 1992, p. 704, pl. 8, figs. 5–8, 17; pl. 9, figs. 24–26; pl. 10, fig. 1; Censarek and Gersonde, 2002, p. 352, pl. 2, figs. 27–31.

S.M. Bohaty et al.
Neogene Diatom and Tephra Stratigraphy

24

Nitzschia grossepunctata Schrader, 1976, pp. 633, 634, pl. 3, figs. 1–4; Harwood and Maruyama, 1992, p. 704, pl. 10, fig. 2; Censarek and Gersonde, 2002, p. 352, pl. 2, figs. 37, 38.

Nitzschia maleinterpretaria Schrader, 1976, p. 634, pl. 2, figs. 9, 11–19, 21, 24.
Synonym: *Fragilariopsis maleinterpretaria* (Schrader) Censarek and Gersonde, 2002, p. 351, pl. 3, fig. 26.

Nitzschia miocenica Burckle; Ciesielski, 1983, p. 656, pl. 2, figs. 9–12; Akiba, 1986, p. 443, pl. 23, figs. 10, 14; Akiba and Yanagisawa, 1986, p. 496, pl. 39, figs. 7–15; pl. 41, figs. 1, 2.
Synonym: *Fragilariopsis miocenica* (Burckle) Censarek and Gersonde, 2002, p. 351.
Remarks: *N. miocenica* is consistently present in upper Miocene samples of Hole 1138A (Table T1).

Nitzschia panduriformis Gregory; Abbott, 1974, p. 316, pl. 11, fig. A.

Nitzschia reinholdii Kanaya ex Schrader, 1973, p. 708, pl. 4, figs. 12–16; pl. 5, figs. 1–9; Akiba, 1986, pp. 443, 444, pl. 22, figs. 4, 5; Akiba and Yanagisawa, 1986, p. 496, pl. 40, figs. 8, 9; pl. 41, figs. 3, 4.
Synonym: *Fragilariopsis reinholdii* (Kanaya) Zielinski and Gersonde, 2002, p. 259, pl. 1, figs. 3, 4; Censarek and Gersonde, 2002, p. 352, pl. 3, figs. 1, 2.

Nitzschia sp. 17 of Schrader, 1976, p. 634, pl. 3, figs. 13–15, 17; pl. 2, fig. 10.

Paralia sulcata (Ehrenberg) Cleve.
Synonym: *Melosira sulcata* (Ehrenberg) Kützing; Schrader, 1973, p. 706, pl. 20, fig. 9.

Porosira pseudodenticulata (Hustedt) Jousé in Kozlova; Krebs, 1983, p. 286, pl. 4, fig. 13.

Radialiplicata clavigera (Grunow) Gleser; Scherer et al., 2000, p. 436, pl. 6, fig. 7.

Raphidodiscus marylandicus Christian; Andrews, 1978, p. 400, pl. 5, figs. 23, 24; Schrader, 1976, p. 635, pl. 5, fig. 19; pl. 15, fig. 16.

Rhabdonema japonicum Tempère and Brun; Scherer et al., 2000, p. 436, pl. 5, fig. 10.

Rhizosolenia costata Gersonde, 1991, pp. 149, 150, pl. 9, figs. 1–6; pl. 10, figs. 1–6; Harwood and Maruyama, 1992, p. 705, pl. 18, figs. 1, 2.

Rhizosolenia hebetata Bailey; Scherer et al., 2000, p. 436, pl. 3, figs. 6, 7.

Rhizosolenia hebetata f. *hiemalis* Gran sensu Schrader, 1973, p. 709, pl. 9, figs. 11, 13–17, 19–21, 24, 25; Schrader, 1976, p. 635, pl. 9, figs. 1–3; Akiba, 1986, p. 444, pl. 17, figs. 10, 11; pl. 18, figs. 9, 10; Harwood and Maruyama, 1992, p. 11, fig. 7.
Remarks: *Rhizosolenia hebetata* f. *hiemalis* and *R. hebetata* f. *hiemalis-spinosa* identified by Schrader (1976) are included together here.

Rhizosolenia styliformis Brightwell; Schrader, 1973, p. 710, pl. 9, fig. 9(?); pl. 10, figs. 1, 18–21.

Rhizosolenia sp. cf. *R. sima* f. *silicea* Sundström; Bohaty et al., 1998, p. 444, pl. 5, figs. 1, 2.
Synonym: *Rhizosolenia* sp. D of Harwood and Maruyama, 1992, p. 705, pl. 18, figs. 7–10; Mahood and Barron, 1996b, p. 292, pl. 1, figs. 4a–5b; pl. 7, fig. 3.
Remarks: See notes regarding this form in Bohaty et al., 1998.

Rocella gelida (Mann) Bukry; Gombos and Ciesielski, 1983, p. 604, pl. 6, figs. 1–6; pl. 26, fig. 1.

Rocella gelida var. *schraderi* (Bukry) Barron, 1983, pp. 511, 512, pl. 4, fig. 10.
Basionym: *Rocella schraderi* Bukry, 1978, p. 788, pl. 6, figs. 1–10; pl. 7, fig. 1; Gombos and Ciesielski, 1983, p. 604, pl. 22, fig. 6.

Rocella praenitida (Fenner) Fenner in Kim and Barron; Harwood and Maruyama, 1992, p. 705, pl. 4, figs. 1–3, 5.

Rocella vigilans var. B of Harwood and Maruyama, 1992, p. 705, pl. 4, figs. 13, 14.

Rouxia antarctica Heiden in Heiden and Kolbe; Schrader, 1976, p. 635, pl. 5, figs. 1–8; Mahood and Barron, 1996b, p. 292, pl. 2, figs. 5, 6; pl. 7, figs. 18, 19; Zielinski and Gersonde, 2002, p. 261, pl. 2, fig. 10.

Rouxia californica Peragallo; Schrader, 1973, p. 710, pl. 3, figs. 18–20, 22(?), 26; Baldauf and Barron, 1991, p. 590, pl. 5, fig. 6.

Rouxia heteropolara Gombos; Gombos, 1977, p. 597, pl. 7, figs. 14, 15.

Rouxia isopolica Schrader, 1976, pp. 635, 636, pl. 5, figs. 9, 14, 15, 20.

Rouxia leventerae Bohaty, Scherer, and Harwood, 1998, pp. 444, 445, pl. 1, figs. 1–6; Zielinski and Gersonde, 2002, p. 261, pl. 2, figs. 1–7.

Rouxia naviculoides Schrader, 1973, p. 710, pl. 3, figs 27–32; Zielinski and Gersonde, 2002, p. 261, pl. 2, figs. 8, 9.

Rouxia peragalli Brun and Héribaud sensu Baldauf and Barron, 1991, p. 590, pl. 5, figs. 7, 8.

Rouxia sp. 1 (Pl. P2, fig. 14; Pl. P3, figs. 7, 8).
   Description and Remarks: *Rouxia* sp. 1 is small (~40 μm in length) with a linear valve outline and rounded ends. The length of each raphe covers approximately one-fourth of the apical length of the valve. This form was noted in three upper Pliocene samples from Hole 1138A.

Spumorbis annulifer Komura, 1998, pp. 5, 6, figs. 17–19, 69–86.

Stellarima microtrias (Ehrenberg) Hasle and Sims; Hasle et al., 1988, pp. 196–198, figs. 1–25.

Stellarima stellaris (Roper) Hasle and Sims; Hasle et al., 1988, pp. 198–200, figs. 26–38.

Synedropsis sp. B
   Synonym: *"Tigeria"* sp. B of Scherer et al., 2000, p. 440, pl. 2, fig. 15 (Pl. P2, fig. 12).

Thalassionema nitzschioides (Grunow) Mereschkowsky; Hasle, 2001, pp. 9–16, figs. 1–3, 5–25, 27.

Thalassionema nitzschioides var. *parvum* Heiden; Hasle, 2001, pp. 9–16, figs. 4, 26.

Thalassionema nitzschioides var. 1
   Description and Remarks: *Thalassionema nitzschioides* var. 1 has one apical end that is inflated. This form is present in the upper Miocene–lower Pliocene section of Hole 1138A.

Thalassiosira antarctica Comber; Krebs, 1983, p. 286, pl. 5, fig. 4a–f; Johansen and Fryxell, 1985, p. 158, figs. 15–17, 37–39.

Thalassiosira bipora Shiono, 2000b, pp. 139–143, figs. 25–44 (Pl. P1, fig. 1).
   Remarks: See discussion under *Thalassiosira tetraoestrupii.*

Thalassiosira complicata Gersonde, 1991, pp. 150, 151, pl. 1, figs. 1, 2; pl. 5, figs. 18–20; pl. 6, figs. 1–6; pl. 7, figs. 1–5.

Thalassiosira sp. cf. *T. eccentrica* (Ehrenberg) Cleve; Fryxell and Hasle, 1972, p. 300, figs. 1–18 (Pl. P1, fig. 6).

Thalassiosira elliptipora (Donahue) Fenner ex Mahood and Barron, 1996b, pp. 292–294, pl. 4, fig. 3; pl. 5, figs. 4a–7c; pl. 8, fig. 6.

S.M. Bohaty et al.
Neogene Diatom and Tephra Stratigraphy

26

Thalassiosira fasciculata Harwood and Maruyama, 1992, p. 707, pl. 15, figs. 4–6; Mahood and Barron, 1996a, p. 287, figs. 15–24, 27, 28.

Thalassiosira gracilis (Karsten) Hustedt; Johansen and Fryxell, 1985, pp. 168–170, figs. 8, 58, 59.

Remarks: *T. gracilis* var. *gracilis* and *T. gracilis* var. *expecta* are grouped together in the present study.

Thalassiosira insigna (Jousé) Harwood and Maruyama, 1992, p. 707, pl. 14, figs. 3–5; Zielinski and Gersonde, 2002, p. 264, pl. 5, figs. 14, 15 (Pl. P1, fig. 4).

Remarks: The current usage of *"Thalassiosira insigna"* for Pliocene specimens from the Southern Ocean is incorrect (D. Harwood, pers. comm., 2002). The basionym for this taxon, *Cosmiodiscus insignis* Jousé, was described from the North Pacific samples (Jousé, 1977) and is better placed within the family Hemidiscaceae, not Thalassiosiraceae, based on the presence of a marginal ring of labiate processes and the absence of strutted processes. The Southern Ocean forms, however, possess strutted processes and, therefore, should be given a separate name within the Thalassiosiraceae (pers. comm. I. Makarova to D. Harwood, 1999). In the current study, we apply the taxonomy of Harwood and Maruyama (1992) and continue the (incorrect) usage of *T. insigna.* Only specimens with an entirely hyaline central area (i.e., nonperforated) are included here as *T. insigna.* Morphologies with a perforated central area are recorded as *Thalassiosira* sp. 1 (see below).

Thalassiosira inura Gersonde, 1991, p. 151, pl. 6, figs. 7–14; pl. 8, figs. 1–6; Gersonde and Burckle, 1990, p. 782, pl. 3, figs. 15–17; pl. 5, fig. 14; Harwood and Maruyama, 1992, p. 707, pl. 14, figs. 12–16.

Thalassiosira jacksonii Koizumi and Barron in Koizumi; Baldauf and Barron, 1991, p. 591, pl. 6, fig. 7.

Thalassiosira kolbei (Jousé) Gersonde, p. 793, pl. 1, fig. 2; pl. 5, figs. 3, 5, 6; Fenner, 1991, p. 108, pl. 1, figs. 1, 4; pl. 2, figs. 3, 4; Mahood and Barron, 1996b, p. 294, pl. 4, figs. 1, 2; pl. 8, fig. 1a, b.

Thalassiosira lentiginosa (Janisch) Fryxell; Mahood and Barron, 1996b, p. 294, pl. 4, figs. 4a, b, 5; pl. 8, fig. 2a, b.

Remarks: The first occurrence of *T. lentiginosa* could not be determined with certainty in Hole 1138A. Early forms of this taxon appear to intergrade with *Thalassiosira striata.* Both *T. lentiginosa* and *T. striata* possess strutted processes that are scattered across the valve face, and some lower to middle Pliocene specimens of *T. striata* possess a large labiate process that is radially oriented on the valve margin—a diagnostic feature of *T. lentiginosa.* SEM work is needed to clarify the taxonomic differences between *T. lentiginosa* and *T. striata.*

Thalassiosira lentiginosa var. *obovatus* (Castracane) Fryxell

Synonym: *Coscinodiscus lentiginosus* f. *obovatus* (Castracane) Ciesielski, 1983, p. 653, pl. 4, figs. 6–8.

Thalassiosira miocenica Schrader; Barron, 1985a, p. 445, pl. 5, fig. 6; Barron, 1985b, p. 792, fig. 11.11; Gersonde and Burckle, 1990, p. 782, pl. 3, figs. 4, 5; Baldauf and Barron, 1991, p. 591, pl. 6, fig. 2.

Thalassiosira nansenii Scherer and Koç, 1996, p. 89, pl. 4, figs. 1–5.

Thalassiosira oliverana (O'Meara) Makarova and Nikolaev; Mahood and Barron, 1996b, pl. 5, figs. 1–3; pl. 8, figs. 3–5.

Remarks: Specimens identified as *T. oliverana* in the present study represent a complex group of morphologies with both coarse and fine areolation. Forms with a central "dimple" (see Harwood and Maruyama, 1992, pl. 14, figs. 11, 17) and small diameter (≤40 μm) are also included here as *T. oliverana.* Specimens of *T. oliverana* var. *sparsa* (see Harwood and Maruyama, 1992, p. 708, pl. 16, fig. 13) were recorded separately (Table T1).

Thalassiosira oliverana var. *sparsa* Harwood and Maruyama, 1992, p. 708, pl. 16, fig. 13; Censarek and Gersonde, 2002, p. 353, pl. 5, figs. 1, 2.

Thalassiosira praefraga Gladenkov and Barron, 1995, pp. 30, 31, pl. 2, figs. 3–6, 9; Scherer et al., 2000, p. 440, pl. 2, figs. 3, 7.

Thalassiosira ritscheri (Hustedt) Hasle; Johansen and Fryxell, 1985, p. 176, figs. 14, 56, 57.

Thalassiosira striata Harwood and Maruyama, 1992, p. 708, pl. 15, figs. 7–9; Zielinski and Gersonde, 2002, p. 264, pl. 4, fig. 7.
Remarks: See discussion under *Thalassiosira lentiginosa.*

Thalassiosira tetraoestrupii Bodén, 1993, p. 63, pl. 1, figs. A–G; pl. 2, figs. A, B, H, J; Mahood and Barron, 1995, figs. 9–19, 25, 26, 28–46.
Remarks: The occurrence chart for the Neogene section of Hole 1138A includes a column identified as the "*Thalassiosira tetraoestrupii* group" (Table T1). This group most likely includes several species that possess a central strutted process and a labiate process on the valve face. *Thalassiosira tetraoestrupii* var. *reimeri* was recorded separately. Several similar species from the broadly defined "*Thalassiosira trifulta* group" have been recently described from Pliocene–Pleistocene sediments of the North Pacific (Shiono, 2000b, 2001). These taxa have not yet been identified in Southern Ocean, but several within this group are most likely present in upper Miocene–lower Pleistocene sediments on the Kerguelen Plateau. Common specimens in Section 183-1138A-8R-5 (see Pl. P1, fig. 1) are tentatively identified as *Thalassiosira bipora* (Shiono, 2000b, pp. 139–143, figs. 25–44), but SEM observations are required to confirm this identification.

Thalassiosira tetraoestrupii var. *reimeri* Mahood and Barron, 1995, p. 2, figs. 1–8, 20–24, 27.
Remarks: *T. tetraoestrupii* var. *reimeri* has a narrow, consistent range in the upper Pliocene of Hole 1138A (Table T1). A few rare specimens, however, were also identified in the lower Pleistocene; these occurrences may indicate a longer total range for this taxon, or they may be reworked.

Thalassiosira torokina Brady, 1977, p. 123, figs. 1–5; Scherer, 1991, pl. 2, fig. 4; Mahood and Barron, 1996b, p. 296, pl. 6, figs. 1–3; pl. 8, fig. 8.
Remarks: Bohaty et al. (1998) describe and illustrate a "late form" of *T. torokina* with a reduced number of central processes from Pleistocene strata recovered in McMurdo Sound, Ross Sea. "Early forms" of *T. torokina* with numerous central processes (Scherer, 1991; Mahood and Barron, 1996b) were observed only in the Pliocene interval of Hole 1138A. "Late forms" of *T. torokina* were not observed in Hole 1138A and, thus, may have been restricted to colder shelf and shelf margin areas during the Pleistocene. It is also possible that these two forms represent separate species.

Thalassiosira trifulta Fryxell in Fryxell and Hasle; Johansen and Fryxell, 1985, p. 176, figs. 12, 65, 66.

Thalassiosira tumida (Janisch) Hasle in Hasle et al.; Fenner et al., 1976, p. 780, pl. 10, figs. 6, 7; Johansen and Fryxell, 1985, pp. 176, 177, figs. 28–32.

Thalassiosira vulnifica (Gombos) Fenner, 1991, p. 108, pl. 2, fig. 2; Mahood and Barron, 1996a, pp. 285–287, figs. 1–14, 25, 26.

Thalassiosira sp. 1 (Pl. P1, fig. 5)
Description and Remarks: *Thalassiosira* sp. 1 is an intermediate form between *T. insigna* and *T. oliverana*. It is characterized by a perforated hyaline central area and the valve diameter is generally smaller than *T. insigna*. A distinctive process between the hyaline area and valve margin is also present on some specimens (Pl. P1, fig. 5). A similar specimen with a perforated hyaline are was referred as *Cosmiodiscus intersectus* (Brun) Jousé by Gersonde and Burckle (1990, p. 780, pl. 4, fig. 13). The Antarctic specimens of *"C. intersectus,"* however, have been put in synonymy with *T. oliverana* var. *sparsa* by Harwood and Maruyama (1992). It is possible that "*Thalassiosira* sp. 1" identified in Hole 1138A is referable to *T. oliverana* var. *sparsa,* but a prominent strutted process outside of the central hyaline area has not been previously documented on *T. oliverana* var. *sparsa* specimens.

Trinacria excavata Heiberg; Gombos and Ciesielski, 1983, p. 605, pl. 17, fig. 8.

ACKNOWLEDGMENTS

REFERENCES

Abbott, W.H., 1974. Temporal and spatial distribution of Pleistocene diatoms from the southeast Indian Ocean. *Nova Hedwigia Beih.,* 25:291–346.

Abelmann, A., Gersonde, R., and Spiess, V., 1990. Pliocene–Pleistocene paleoceanography in the Weddell Sea: siliceous microfossil evidence. *In* Bleil, U., and Thiede, J. (Eds.), *Geologic History of the Polar Oceans: Arctic Versus Antarctic:* NATO ASI Ser., Ser. C, 308:729–759.

Akiba, F., 1982. Late Quaternary diatom biostratigraphy of the Bellingshausen Sea, Antarctic Ocean. *Rep. Tech. Res., Cen. Jpn. Nat. Oil Corp.,* 16:31–74.

Akiba, F., 1986. Middle Miocene to Quaternary diatom biostratigraphy in the Nankai trough and Japan trench, and modified lower Miocene through Quaternary diatom zones for middle-to-high latitudes of the North Pacific. *In* Kagami, H., Karig, D.E., Coulbourn, W.T., et al., *Init. Repts. DSDP,* 87: Washington (U.S. Govt. Printing Office), 393–481.

Akiba, F., Hiramatsu, C., and Yanagisawa,Y., 1993. A Cenozoic diatom genus *Cavitatus* Williams; an emended description and two new biostratigraphically useful species, *C. lanceolatus* and *C. rectus* from Japan. *Bull. Nat. Sci. Mus. Ser. C.: Geol. Paleontol. (Tokyo),* 19:11–39.

Akiba, F., and Yanagisawa, Y., 1986. Taxonomy, morphology and phylogeny of the Neogene diatom zonal marker species in the middle-to-high latitudes of the North Pacific. *In* Kagami, H., Karig, D.E., Coulbourn, W.T., et al., *Init. Repts. DSDP,* 87: Washington (U.S. Govt. Printing Office), 483–554.

Andrews, G.W., 1978. Marine diatom sequence in Miocene strata of the Chesapeake Bay region, Maryland. *Micropaleontology,* 24:371–406.

Baldauf, J.G., 1985. A high resolution late Miocene–Pliocene diatom biostratigraphy for the eastern equatorial Pacific. *In* Mayer, L., Theyer, F., Thomas, E., et al., *Init. Repts. DSDP,* 85: Washington (U.S. Govt. Printing Office), 457–475.

Baldauf, J.G., and Barron, J.A., 1980. *Actinocyclus ingens* var. *nodus:* a new stratigraphically useful diatom of the circum-North Pacific. *Micropaleontology,* 26:103–110.

————, 1991. Diatom biostratigraphy: Kerguelen Plateau and Prydz Bay regions of the Southern Ocean. *In* Barron, J., Larsen, B., et al., *Proc. ODP, Sci. Results,* 119: College Station, TX (Ocean Drilling Program), 547–598.

Baldauf, J.G., and Iwai, M., 1995. Neogene diatom biostratigraphy for the eastern equatorial Pacific Ocean, Leg 138. *In* Pisias, N.G., Mayer, L.A., Janecek, T.R., Palmer-Julson, A., and van Andel, T.H. (Eds.), *Proc. ODP, Sci. Results,* 138: College Station, TX (Ocean Drilling Program), 105–128.

Barker, P.F., Camerlenghi, A., Acton, G.D., et al., 1999. *Proc. ODP, Init. Repts.,* 178 [Online]. Available from World Wide Web: <http://www-odp.tamu.edu/publications/178_IR/178TOC.HTM>. [Cited 2003-03-10]

Barron, J.A., 1983. Latest Oligocene through early middle Miocene diatom biostratigraphy of the eastern tropical Pacific. *Mar. Micropaleontol.,* 7:487–515.

————, 1985a. Late Eocene to Holocene diatom biostratigraphy of the equatorial Pacific Ocean, Deep Sea Drilling Project Leg 85. *In* Mayer, L., Theyer, F., Thomas, E., et al., *Init. Repts. DSDP,* 85: Washington (U.S. Govt. Printing Office), 413–456.

————, 1985b. Miocene to Holocene planktic diatoms. *In* Bolli, H.M., Saunders, J.B., and Perch-Nielsen, K. (Eds.), *Plankton Stratigraphy:* Cambridge (Cambridge Univ. Press), 763–809.

Barron, J.A., Baldauf, J.G., Barrera, E., Caulet, J.-P., Huber, B.T., Keating, B.H., Lazarus, D., Sakai, H., Thierstein, H.R., and Wei, W., 1991. Biochronologic and magnetochronologic synthesis of Leg 119 sediments from the Kerguelen Plateau and Prydz Bay, Antarctica. *In* Barron, J., Larsen, B., et al., *Proc. ODP, Sci. Results,* 119: College Station, TX (Ocean Drilling Program), 813–847.

Berggren, W.A., Kent, D.V., Swisher, C.C., III, and Aubry, M.-P., 1995. A revised Cenozoic geochronology and chronostratigraphy. *In* Berggren, W.A., Kent, D.V., Aubry,

M.-P., and Hardenbol, J. (Eds.), *Geochronology, Time Scales and Global Stratigraphic Correlation.* Spec. Publ.—SEPM, 54:129–212.

Bodén, P., 1993. Taxonomy and stratigraphic occurrence of *Thalassiosira tetraoestrupii* sp. nov. and related species in upper Miocene and lower Pliocene sediments from the Norwegian Sea, North Atlantic and northwest Pacific. *Terra Nova,* 5:61–75.

Bohaty, S.M., and Harwood, D.M., 1998. Southern Ocean Pliocene paleotemperature variation from high-resolution silicoflagellate biostratigraphy. *Mar. Micropal.,* 33:241–272.

Bohaty, S.M., Scherer, R.P., and Harwood, D.M., 1998. Quaternary diatom biostratigraphy and palaeoenvironments of the CRP-1 drillcore, Ross Sea, Antarctica. *Terra Antart.,* 5:431–453.

Brady, H.T., 1977. *Thalassiosira torokina* n. sp. (diatom) and its significance in late Cenozoic biostratigraphy. *Antarct. J. U.S.,* 12:122–123.

Bukry, D., 1978. Cenozoic silicoflagellate and coccolith stratigraphy, northwestern Atlantic Ocean, Deep Sea Drilling Project Leg 43. *In* Bensen, W.E., Sheridan, R.E., et al., *Init. Repts. DSDP,* 44: Washington (U.S. Govt. Printing Office), 775–805.

Burckle, L.H., Clarke, D.B., and Shackleton, N.J., 1978. Isochronous last-abundant-appearance datum (LAAD) of the diatom *Hemidiscus karstenii* in the sub-Antarctic. *Geology,* 6:243–246.

Cas, R.A.F., and Wright, J.V., 1988. *Volcanic Successions Modern and Ancient:* London (Allen and Unwin), 99–104.

Censarek, B., and Gersonde, R., 2002. Miocene diatom biostratigraphy at ODP Sites 689, 690, 1088, 1092 (Atlantic sector of the Southern Ocean). *Mar. Micropaleontol.,* 45:309–356.

Ciesielski, P.F., 1983. The Neogene and Quaternary diatom biostratigraphy of subantarctic sediments, Deep Sea Drilling Project Leg 71. *In* Ludwig, W.J., Krasheninnikov, V.A., et al., *Init. Repts. DSDP,* 71 (Pt. 2): Washington (U.S. Govt. Printing Office), 635–666.

————, 1986. Middle Miocene to Quaternary diatom biostratigraphy of Deep Sea Drilling Project Site 594, Chatham Rise, southwest Pacific. *In* Kennett. J.P., von der Borch, C.C., et al., *Init. Repts. DSDP,* 90 (Pt. 2): Washington (U.S. Govt. Printing Office), 863–885.

Coffin, M.F., Frey, F.A., Wallace, P.J., et al., 2000. *Proc. ODP, Init. Repts.,* 183 [Online]. Available from World Wide Web: <http://www-odp.tamu.edu/publications/183_IR/183ir.htm>. [2000-08-01]

Dalrymple, G.B., Alexander, E.C., Lanphere, M.A., and Kraker, G.P., 1981. *Irradiation of Samples for $^{40}Ar/^{39}Ar$ Dating Using the Geological Survey TRIGA Reactor.* Geol. Surv. Prof. Pap. U.S., 1176.

Dalrymple, G.B., Lanphere, M.A., and Clague, D.A., 1980. Conventional and $^{40}Ar/^{39}Ar$ K-Ar ages of volcanic rocks from Ojin (Site 430), Nintoku (Site 432) and Suiko (Site 433) seamounts and the chronology of volcanic propagation along the Hawaiian-Emperor Chain. *In* Jackson, E.D., Koizumi, I., et al., *Init. Repts. DSDP,* 55: Washington (U.S. Govt. Printing Office), 659–676.

Fenner, J., Schrader, H.-J., and Wienigk, H., 1976. Diatom phytoplankton studies in the southern Pacific Ocean: composition and correlation to the Antarctic Convergence and its paleoecological significance. *In* Hollister, C.D., Craddock, C., et al., *Init. Repts. DSDP,* 35: Washington (U.S. Govt. Printing Office), 757–813.

Fenner, J.M., 1991. Late Pliocene–Quaternary quantitative diatom stratigraphy in the Atlantic sector of the Southern Ocean. *In* Ciesielski, P.F., Kristoffersen, Y., et al., *Proc. ODP, Sci. Results,* 114: College Station, TX (Ocean Drilling Program), 97–121.

Frey, F.A., Coffin, M.F., Wallace, P.J., Weis, D., Zhao, X., et al., 2000. Origin and evolution of a submarine large igneous province: the Kerguelen Plateau and Broken Ridge, southern Indian Ocean. *Earth Planet. Sci. Lett.,* 176:73–89.

Fryxell, G.A., and Hasle, G.R., 1972. *Thalassiosira eccentrica* (Ehrenberg) Cleve, *T. symmetrica* sp. nov., and some related Centric diatoms. *J. Phycol.,* 8:297–317.

Fryxell, G.A., Sims, P.A., and Watkins, T.P., 1986. *Azpeitia* (Bacillariophyceae): related genera and promorphology. *Syst. Bot. Monogr.,* 13:1–74.

Gersonde, R., 1990. Taxonomy and morphostructure of Neogene diatoms from the Southern Ocean, ODP Leg 113. *In* Barker, P.F., Kennett, J.P., et al., *Proc. ODP, Sci. Results,* 113: College Station, TX (Ocean Drilling Program), 791–802.

————, 1991. Taxonomy and morphostructure of late Neogene diatoms from Maud Rise (Antarctic Ocean). *Polarforschung,* 59:141–171.

Gersonde, R., and Bárcena, M.A., 1998. Revision of the late Pliocene–Pleistocene diatom biostratigraphy for the northern belt of the Southern Ocean. *Micropaleontology,* 44:84–98.

Gersonde, R., and Burckle, L.H., 1990. Neogene diatom biostratigraphy of ODP Leg 113, Weddell Sea (Antarctic Ocean). *In* Barker, P.F., Kennett, J.P., et al., *Proc. ODP, Sci. Results,* 113: College Station, TX (Ocean Drilling Program), 761–789.

Gersonde, R., and Zielinski, U., 2000. The reconstruction of late Quaternary Antarctic sea-ice distribution—the use of diatoms as a proxy for sea-ice. *Palaeogeogr., Palaeoclimatol., Palaeoecol.,* 162:263–286.

Gladenkov, A.Y., and Barron, J.A., 1995. Oligocene and early middle Miocene diatom biostratigraphy of Hole 884B. *In* Rea, D.K., Basov, I.A., Scholl, D.W., and Allan, J.F. (Eds.), *Proc. ODP, Sci. Results,* 145: College Station, TX (Ocean Drilling Program), 21–41.

Gombos, A.M., Jr., 1977. Paleogene and Neogene diatoms from the Falkland Plateau and Malvinas Outer Basin: Leg 36, Deep Sea Drilling Project. *In* Barker, P., Dalziel, I.W.D., et al., *Init. Repts. DSDP,* 36: Washington (U.S. Govt. Printing Office), 575–690.

Gombos, A.M., Jr., and Ciesielski, P.F., 1983. Late Eocene to early Miocene diatoms from the southwest Atlantic. *In* Ludwig, W.J., Krasheninnikov, V.A., et al., *Init. Repts. DSDP,* 71 (Pt. 2): Washington (U.S. Govt. Printing Office), 583–634.

Harwood, D.M., 1991. Cenozoic diatom biogeography in the southern high latitudes: inferred biogeographic barriers and progressive endemism. *In* Thomson, M.R.A., Crame, J.A., Thomson, J.W. (Eds.), *Proc. 5th Int. Symp. Antarct. Earth Sci.:* New York (Cambridge Univ. Press) 5:667–673.

Harwood, D.M., Lazarus, D.B., Abelmann, A., Aubry, M.-P., Berggren, W.A., Heider, F., Inokuchi, H., Maruyama, T., McCartney, K., Wei, W., and Wise, S.W., Jr., 1992. Neogene integrated magnetobiostratigraphy of the central Kerguelen Plateau, Leg 120. *In* Wise, S.W., Jr., Schlich, R., et al., *Proc. ODP, Sci. Results,* 120: College Station, TX (Ocean Drilling Program), 1031–1052.

Harwood, D.M., and Maruyama, T., 1992. Middle Eocene to Pleistocene diatom biostratigraphy of Southern Ocean sediments from the Kerguelen Plateau, Leg 120. *In* Wise, S.W., Jr., Schlich, R., et al., *Proc. ODP, Sci. Results,* 120: College Station, TX (Ocean Drilling Program), 683–733.

Harwood, D.M., McMinn, A., and Quilty, P.G., 2000. Diatom biostratigraphy and age of the Pliocene Sørsdal Formation, Vestfold Hills, East Antarctica. *Antarctic Sci.,* 12:443–462.

Hasle, G.R., 1965. *Nitzschia* and *Fragilariopsis* species in the light and electron microscopes. III. The genus *Fragilariopsis*. *Skr. Nor. Vidensk.-Akad. Kl. 1: Mat.-Naturvidensk Kl.,* 21:5–49.

————, 1972. *Fragilariopsis* Hustedt as a section of the genus *Nitzschia* Hassal. *Beiheft zur Nova Hedwigia,* 39:111–119.

————, 1974. Validation of the names of some marine planktonic species of *Nitzschia* (Bacillariophyceae). *Taxon,* 23:425–428.

————, 1975. Some living marine species of the diatom family Rhizosoleniaceae. *Nova Hedwigia Beih.,* 53:99–153.

————, 2001. The marine, planktonic diatom family *Thalasionemataceae:* morphology, taxonomy and distribution. *Diatom Res.,* 16:1–82.

Hasle, G.R., and Medlin, L.K., 1990. Chapter 24: Family Bacillariaceae: Genus *Nitzschia,* section *Fragilariopsis. In* Medlin, L.K., and Priddle, J. (Eds.), *Polar Marine Diatoms.* Br. Antarct. Surv., 181–196.

Hasle, G.R., Sims, P.A., and Syvertsen, E.E., 1988. Two recent *Stellerima* species: *S. microtrias* and *S. stellaris* (Bacillariophyceae). *Bot. Mar.,* 31:195–206.

Hasle, G.R., and Syvertsen, E.E., 1996. Marine diatoms. *In* Tomas, C.R. (Ed.), *Identifying Marine Diatoms and Dinoflagellates:* New York (Academic Press), 5–386.

Heider, F., Leitner, B., and Inokuchi, H., 1992. High southern latitude magnetostratigraphy and rock magnetic properties of sediments from Sites 747, 749, and 751. *In* Wise, S.W., Jr., Schlich, R., et al., *Proc. ODP, Sci. Results,* 120: College Station, TX (Ocean Drilling Program), 225–245.

Hendy, N.I., 1981. Miocene diatoms from the subantarctic southwest Pacific, DSDP Leg 29, Site 278, Core 10. *Bacillaria,* 4:65–124.

Johansen, J.R., and Fryxell, G.A., 1985. The genus *Thalassiosira* (Bacillariophyceae): studies on species occurring south of the Antarctic Convergence Zone. *Phycologia,* 24:155–179.

Jousé, A.P., 1977. *Atlas of Microorganisms in Bottom Sediments of the Oceans (Diatoms, Radiolaria, Silicoflagellates and Coccoliths):* Moscow (NAUKA). [In Russian].

Koizumi, I., 1973. The late Cenozoic diatoms of Sites 183–193, Leg 19 Deep Sea Drilling Project. *In* Creager, J.S., Scholl, D.W., et al., *Init. Repts. DSDP,* 19: Washington (U.S. Govt. Printing Office), 805–855.

Komura, S., 1998. A perplexing morphotype of some centric diatoms inclusive of *Coscinodiscus lewisianus* Grev. and its allies. *Diatom,* 14:1–23.

Koppers, A.A.P., 2002. ArArCALC: software for $^{40}Ar/^{39}Ar$ age calculations. *Comput. Geosci.,* 28:605–619.

Krebs, W.N., 1983. Ecology of neritic marine diatoms, Arthur Harbor, Antarctica. *Micropaleontology,* 29:267–297.

Lohman, K.E., 1938. Pliocene diatoms from the Kettleman Hills, California. *Geol. Surv. Prof. Pap. U.S.,* 189-C:81–102.

Mahood, A.D., and Barron, J.A., 1995. *Thalassiosira tetraoestrupii* var. *reimeri* var. nov., a distinctive diatom from the late Pliocene of the Southern Ocean. *In* Kociolek, J.P., and Sullivan, M.J. (Eds.), A *Century of Diatom Research in North America: A Tribute to the Distinguished Careers of Charles Reimer and Ruth Patrick:* Champaign, IL (Koeltz Sci. Books USA), 1–8.

————, 1996a. Comparitive ultrastructure of two closely related *Thalassiosira* species: *Thalassiosira vulnifica* (Gombos) Fenner and *T. fasciculata* Harwood et Maruyama. *Diatom Res.,* 11:283–295.

————, 1996b. Late Pliocene diatoms in a diatomite from Prydz Bay, East Antarctica. *Micropaleontology,* 42:285–302.

McCollum, D.W., 1975. Diatom stratigraphy of the southern Ocean. *In* Hayes, D.E., Frakes, L.A., et al., *Init. Repts. DSDP,* 28: Washington (U.S. Govt. Printing Office), 515–571.

McDougall, I., and Harrison, T.M., 1999. *Geochronology and Thermochronology by the $^{40}Ar/^{39}Ar$ Method* (2nd ed.): Oxford (Oxford Univ. Press).

McMinn, A., Howard, W.R., and Roberts, D., 2001. Late Pliocene dinoflagellate cyst and diatom analysis from a high resolution sequence in DSDP Site 594, Chatham Rise, southwest Pacific. *Mar. Micropaleontol.,* 43:207–221.

Medlin, L.K., and Sims, P.A., 1993. The transfer of *Pseudoeunotia doliolus* to *Fragilariopsis. Nova Hedwigia Beih.,* 106:323–334.

Morche, W., Hubberten, H.-W., Ehrmann, W.U., and Keller, J., 1991. Geochemical investigations of volcanic ash layers from Leg 119, Kerguelen Plateau. *In* Barron, J., Larsen, B., et al., *Proc. ODP, Sci. Results,* 119: College Station, TX (Ocean Drilling Program), 323–346.

Morche, W., Hubberten, H.-W., Mackensen, A., and Keller, J., 1992. Geochemistry of Cenozoic ash layers from the Kerguelen Plateau (Leg 120): a first step toward a tephrostratigraphy of the southern Indian Ocean. *In* Wise, S.W., Jr., Schlich, R., et

al., *Proc. ODP, Sci. Results,* 120: College Station, TX (Ocean Drilling Program), 151–160.

O'Brien, P.E., Cooper, A.K., Richter, C., et al., 2001. *Proc. ODP, Init. Repts.,* 188 [Online]. Available from World Wide Web: <http://www-odp.tamu.edu/publications/188_IR/188ir.htm>. [2001-05-01]

Pringle, M.S., and Duncan, R.A., 1995. Radiometric ages of basement lavas recorded at Loen, Wodejebato, MIT, and Takuyo-Daisan. *In* Haggerty, J.A., Premoli Silva, I., Rack, F., and McNutt, M.K. (Eds.), *Proc. ODP, Sci. Results,* 144: College Station, TX (Ocean Drilling Program), 547–557.

Ramsay, A.T.S., and Baldauf, J.G., 1999. A reassessment of the Southern Ocean biochronology. *Mem.—Geol. Soc. Am.,* 18:1–122.

Renne, P.R., Deino, A.L., Walter, R.C., Turrin, B.D., Swisher, C.C., Becker, T.A., Curtis, G.H., Sharp, W.D., and Jaouni, A.-R., 1994. Intercalibration of astronomical and radioisotopic time. *Geology,* 22:783–786.

Scherer, R.P., 1991. Quaternary and Tertiary microfossils from beneath Ice Stream B: evidence for a dynamic West Antarctic Ice Sheet history. *Palaeogeogr., Palaeoclimatol., Palaeoecol.,* 90:395–412.

Scherer, R.P., Bohaty, S.M., Harwood, D.M., 2000. Oligocene and lower Miocene siliceous microfossil biostratigraphy of Cape Roberts project Core CRP-2/2A, Victoria Land Basin, Antarctica. *Terra Antarct.,* 7:417–442.

Scherer, R.P., and Koç, N., 1996. Late Paleogene diatom biostratigraphy and paleoenvironments of the northern Norwegian-Greenland Sea. *In* Thiede, J., Myhre, A.M., Firth, J.V., Johnson, G.L., and Ruddiman, W.F. (Eds.), *Proc. ODP, Sci. Results,* 151: College Station, TX (Ocean Drilling Program), 75–99.

Schlich, R., Wise, S.W., Jr., et al., 1989. *Proc. ODP, Init. Repts.,* 120: College Station, TX (Ocean Drilling Program).

Schrader, H.-J., 1973. Cenozoic diatoms from the Northeast Pacific, Leg 18. *In* Kulm, L.D., von Huene, R., et al., *Init. Repts. DSDP,* 18: Washington (U.S. Govt. Printing Office), 673–797.

————, 1976. Cenozoic planktonic diatom biostratigraphy of the Southern Pacific Ocean. *In* Hollister, C.D., Craddock, C., et al., *Init. Repts. DSDP,* 35: Washington (U.S. Govt. Printing Office), 605–671.

Schrader, H.-J., and Fenner, J., 1976. Norwegian Sea Cenozoic diatom biostratigraphy and taxonomy. *In* Talwani, M., Udintsev, G., et al., *Init. Repts. DSDP,* 38: Washington (U.S. Govt. Printing Office), 921–1099.

Shiono, M., 2000a. The characteristic evolution of the centric diatom: the *Thalassiosira trifulta* group and the *Azpeitia nodulifera* group in Neogene sediments from the northwest Pacific Ocean [Ph.D. thesis]. Hokkaido Univ., Japan, 1–181.

————, 2000b. Three new species in the *Thalassiosira trifulta* group in late Neogene sediments from the northwest Pacific Ocean. *Diatom Res.,* 15:131–148.

————, 2001. Two new species of the *Thalassiosira trifulta* group in late Pliocene sediments of the northwest Pacific Ocean. *Diatom Res.,* 16:83–92.

Shiono, M., and Koizumi, I., 2002. Taxonomy of the *Azpeitia nodulifera* group in late Neogene sediments from the northwest Pacific Ocean. *Diatom Res.,* 17:337–362.

Simonsen, R., 1982. Notes on the diatom genus *Charcotia* M. Peragallo. *Bacillaria,* 5:101–116.

Van Heurck, H., 1909. Expedition Antarctique Belge. *Resultats du Voyage du S.Y. "Belgica" en 1897–1899,* Botanique, Diatomees. Anvers (J. E. Buschmann).

Villareal, T.A., and Fryxell, G.A., 1983. The genus *Actinocyclus* (Bacillariophyceae): frustule morphology of *A. sagittulus* sp. nov. and two related species. *J. Phycol.,* 19:452–466.

Wallace, P., 2002. Volatiles in submarine basaltic glasses from the Northern Kerguelen Plateau (ODP Site 1140): implications for source region compositions, magmatic processes, and plateau subsidence. *J. Petrol.,* 43:1311–1326.

Weaver, F.M., and Gombos, A.M., 1981. Southern high-latitude diatom biostratigraphy. *In* Warme, T.E., Douglas, R.G., and Winterer, E.L. (Eds.), *The Deep Sea Drilling Project: A Decade of Progress:* Spec. Publ.—SEPM, 32:445–470.

Wei, W., and Wise, S.W., Jr., 1992. Oligocene–Pleistocene calcareous nannofossils from Southern Ocean Sites 747, 748, and 751. *In* Wise, S.W., Jr., Schlich, R., et al., *Proc. ODP, Sci. Results,* 120: College Station, TX (Ocean Drilling Program), 509–521.

Winter, D., and Iwai, M., 2002. Data report: Neogene diatom biostratigraphy, Antarctic Peninsula Pacific margin, ODP Leg 178 rise sites. *In* Barker, P.F., Camerlenghi, A., Acton, G.D., and Ramsay, A.T.S. (Eds.), *Proc. ODP, Sci. Results,* 178 [Online]. Available from World Wide Web: <http://www-odp.tamu.edu/publications/178_SR/chap_29/chap_29.htm>. [2002-06-01]

Winter, D.M., and Harwood, D.M., 1997. Integrated diatom biostratigraphy of late Neogene drillholes in Southern Victoria Land and correlation to Southern Ocean records. *In* Ricci, C.A. (Ed.), *The Antarctic Region: Geological Evolution and Processes.* Terra Antart. Publ., 985–992.

Wise, S.W., Gombos, A.M., and Muza, J.P., 1985. Cenozoic evolution of polar water masses, southwest Atlantic Ocean. *In* Hsü, K.J., and Weissert, H.J. (Eds.), *South Atlantic Paleoceanography:* Cambridge (Cambridge Univ. Press), 283–324.

Wright, J.D., and Miller, K.G., 1993. Southern Ocean influences on Late Eocene to Miocene deep-water circulation. *In* Kennett, J.P., and Warnke, D.A. (Eds.), *The Antarctic Paleoenvironment: A Perspective on Global Change.* Antarct. Res. Ser., 60:1–25.

Yanagisawa, Y., 1995. Cenozoic diatom genus *Rossiella* Desikachary et Maheshwari: an emended description. *Trans. Proc. Palaeontol. Soc. Jpn., New Ser.,* 177:1–20.

Yanagisawa, Y., and Akiba, F., 1990. Taxonomy and phylogeny of the three marine diatom genera, *Crucidenticula, Denticulopsis* and *Neodenticula. Bull. Geol. Surv. Jpn.,* 41:197–301.

————, 1998. Refined Neogene diatom biostratigraphy for the northwest Pacific around Japan, with an introduction of code numbers for selected diatom biohorizons. *J. Geol. Soc. Jpn.,* 104:395–414.

Zachos, J.C., Shackleton, N.J., Revenaugh, J.S., Pälike, H., and Flower, B.P., 2001. Climate response to orbital forcing across the Oligocene-Miocene boundary. *Science,* 292:274–278.

Zielinski, U., and Gersonde, R., 2002. Plio–Pleistocene diatom biostratigraphy from ODP Leg 177, Atlantic sector of the Southern Ocean. *Mar. Micropaleontol.,* 45:225–268.

Figure F1. Location of ODP Sites 747 and 1138, Central Kerguelen Plateau.
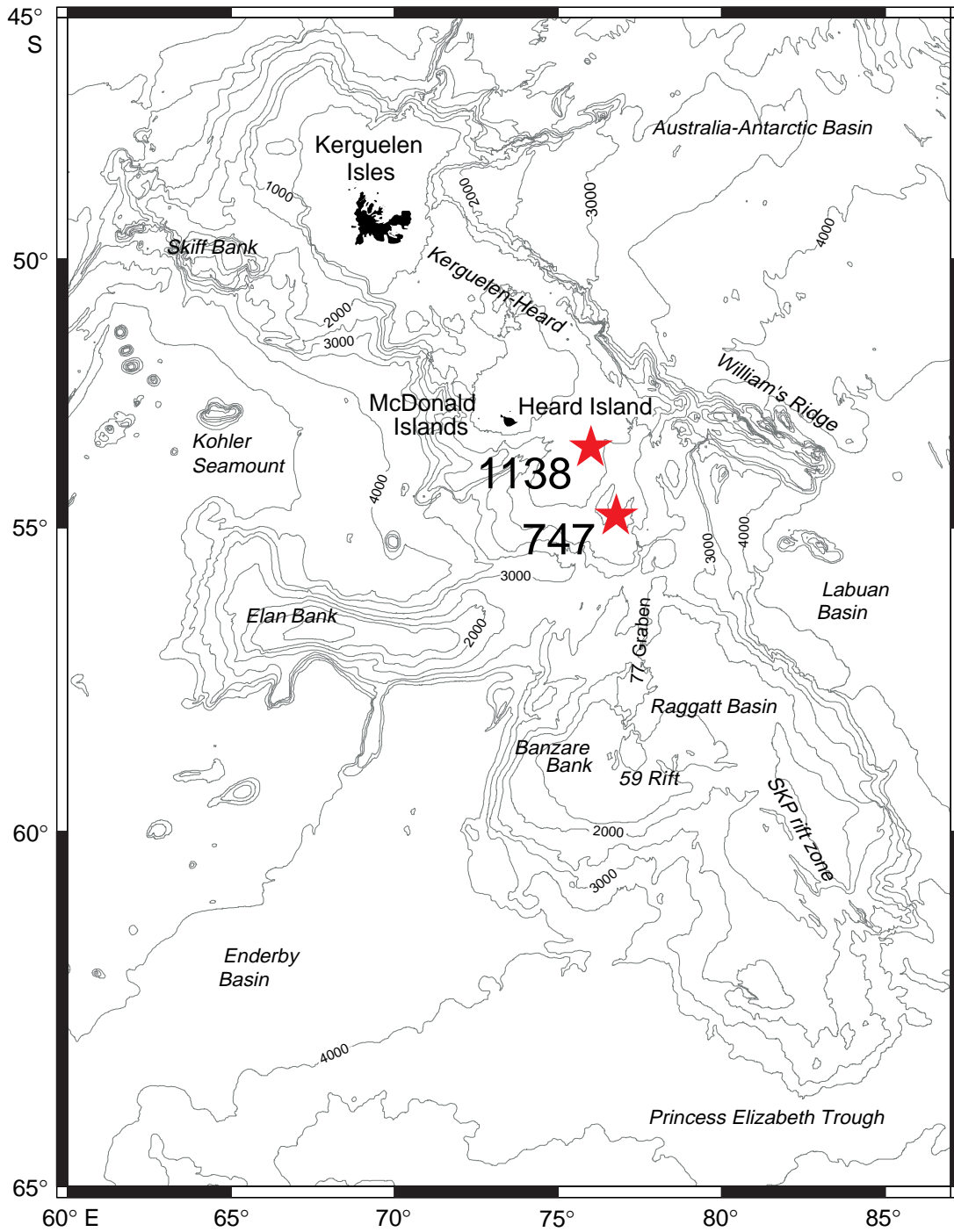
Figure F2. Neogene recovery, lithologic units, tephra horizons, and relative diatom and nannofossil abundance, Hole 1138A. Abundance estimates: B = Barren, X = present, R = rare, F = few, C = common, and A = abundant. Red horizontal bars in tephra column = positions of tephra horizons identified in shipboard core descriptions (Coffin, Frey, Wallace, et al., 2000), * = tephra horizons considered in this study.
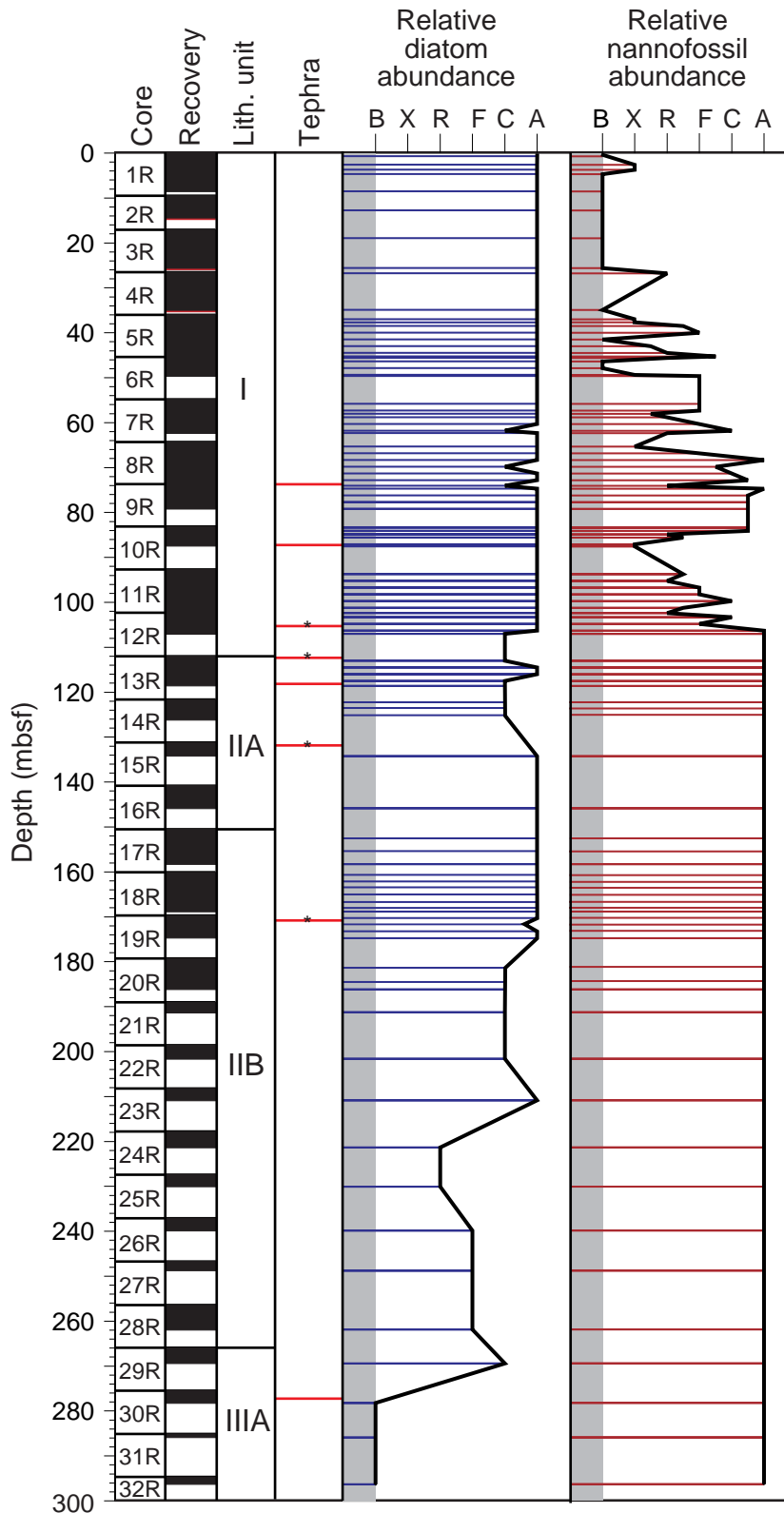
Figure F3. A. Diatom zonal scheme applied to strata of ODP Hole 1138A, 0–15 Ma (modified from Harwood and Maruyama, 1992). Brackets = first or last occurrence datums, and solid triangles = first common or last common occurrence datums. (Continued on next page.)
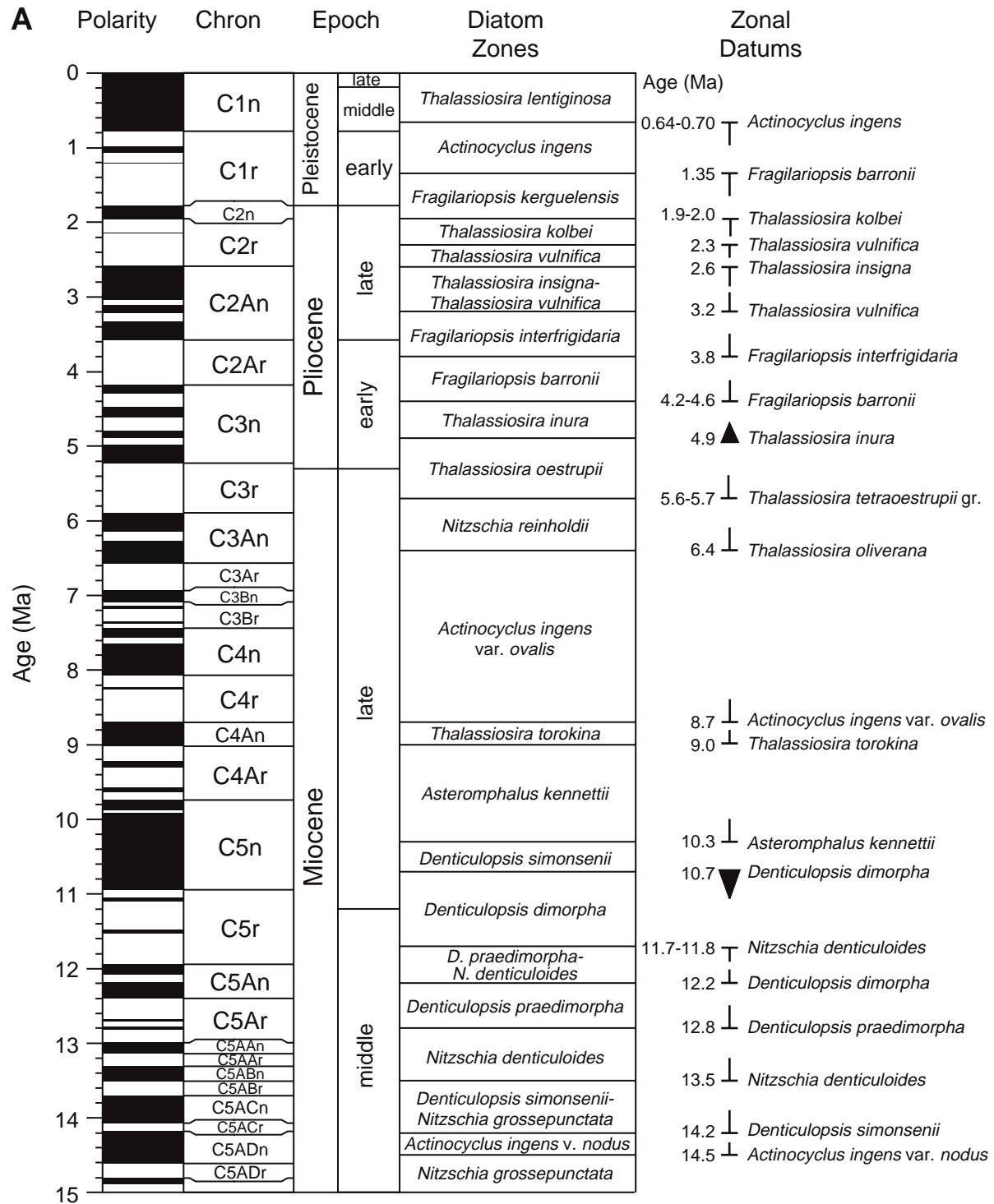
Figure F3 (continued). B. Diatom zonal scheme applied to strata of ODP Hole 1138A, 15–28 Ma.
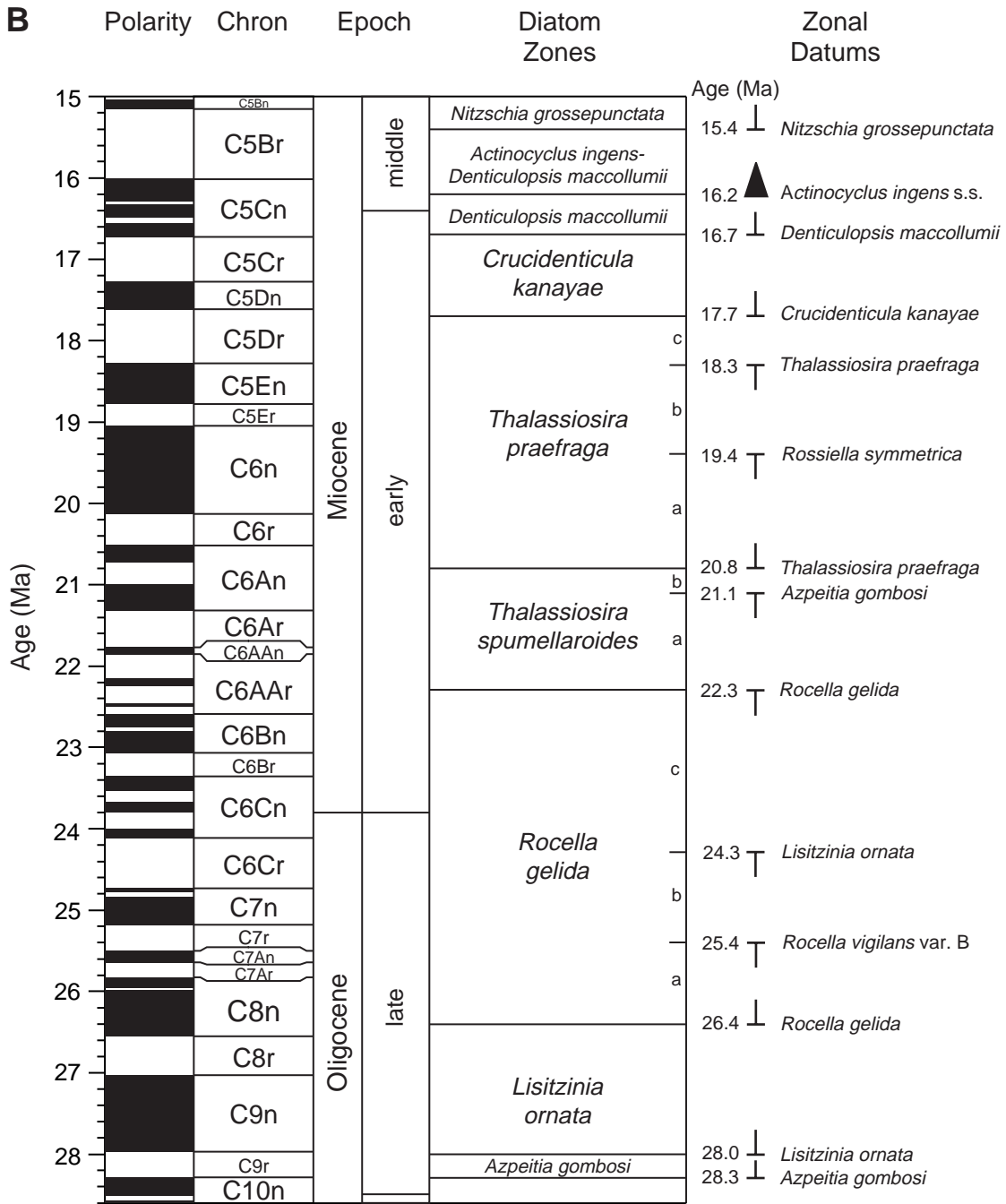
Figure F4. Total alkalis (Na$_2$O + K$_2$O) vs. SiO$_2$ classification plot showing data for glass shards in Site 1138 tephra (solid symbols) and igneous rocks recovered by drilling on the Kerguelen Plateau and Broken Ridge (open symbols). Glass shard analyses were determined by electron microprobe as discussed in the text; all analyses were recalculated to a sum of 100% for plotting purposes. Sources for igneous rock data are given in Frey et al. (2000).
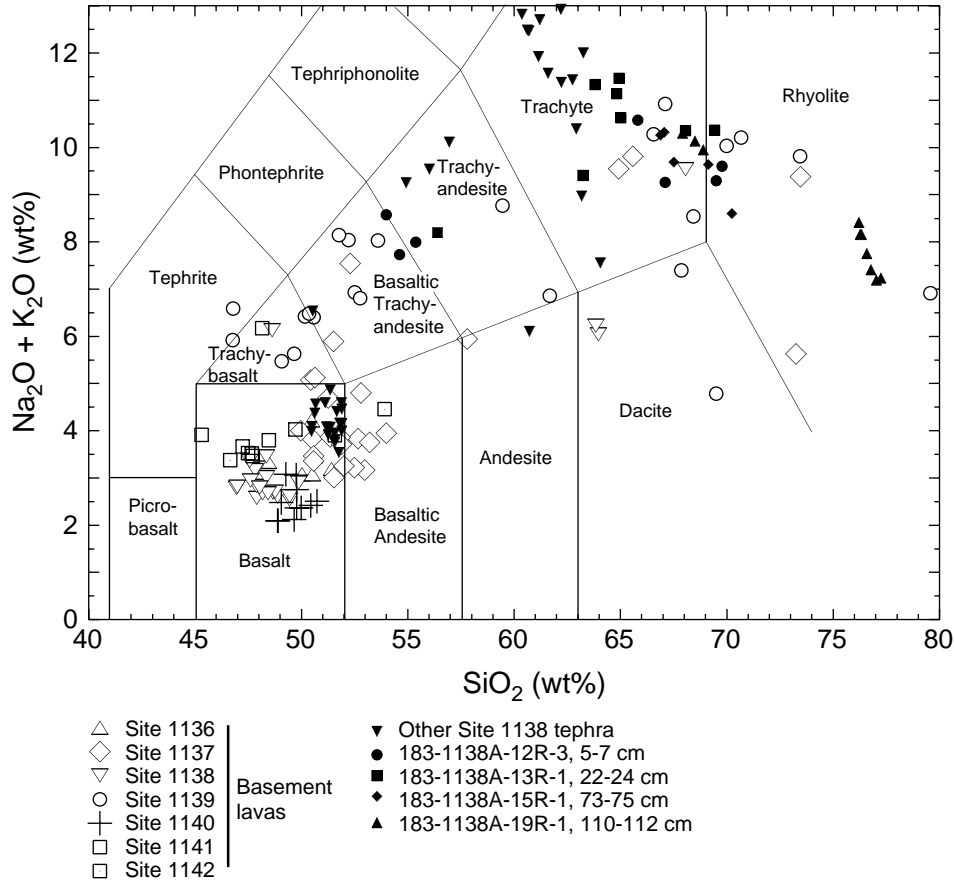
Figure F5. Age plateau and isochron diagrams for ^{40}Ar-^{39}Ar incremental heating experiments, performed at Oregon State University, for ODP Hole 1138A ash layers. Plateau ages are the weighted means of consecutive, concordant step ages constituting at least 50% of the total gas released during incremental heating experiments; isochron ages are determined from least-squares regression of collinear step compositions. The ^{40}Ar-^{39}Ar intercept value gives the Ar composition in the mineral/glass at the time of crystallization. **A.** Sample 183-1138A-12R-3, 5–7 cm (glass). **B.** Sample 183-1138A-13R-1, 22–24 cm (biotite). **C.** Sample 183-1138A-15R-1, 73–75 cm (glass). **D.** Sample 183-1138A-19R-1, 110–112 cm (glass). **E.** Sample 183-1138A-19R-1, 110–112 cm (biotite). Calculations and plots were produced using ArArCALC (version 21) by Koppers (2002).
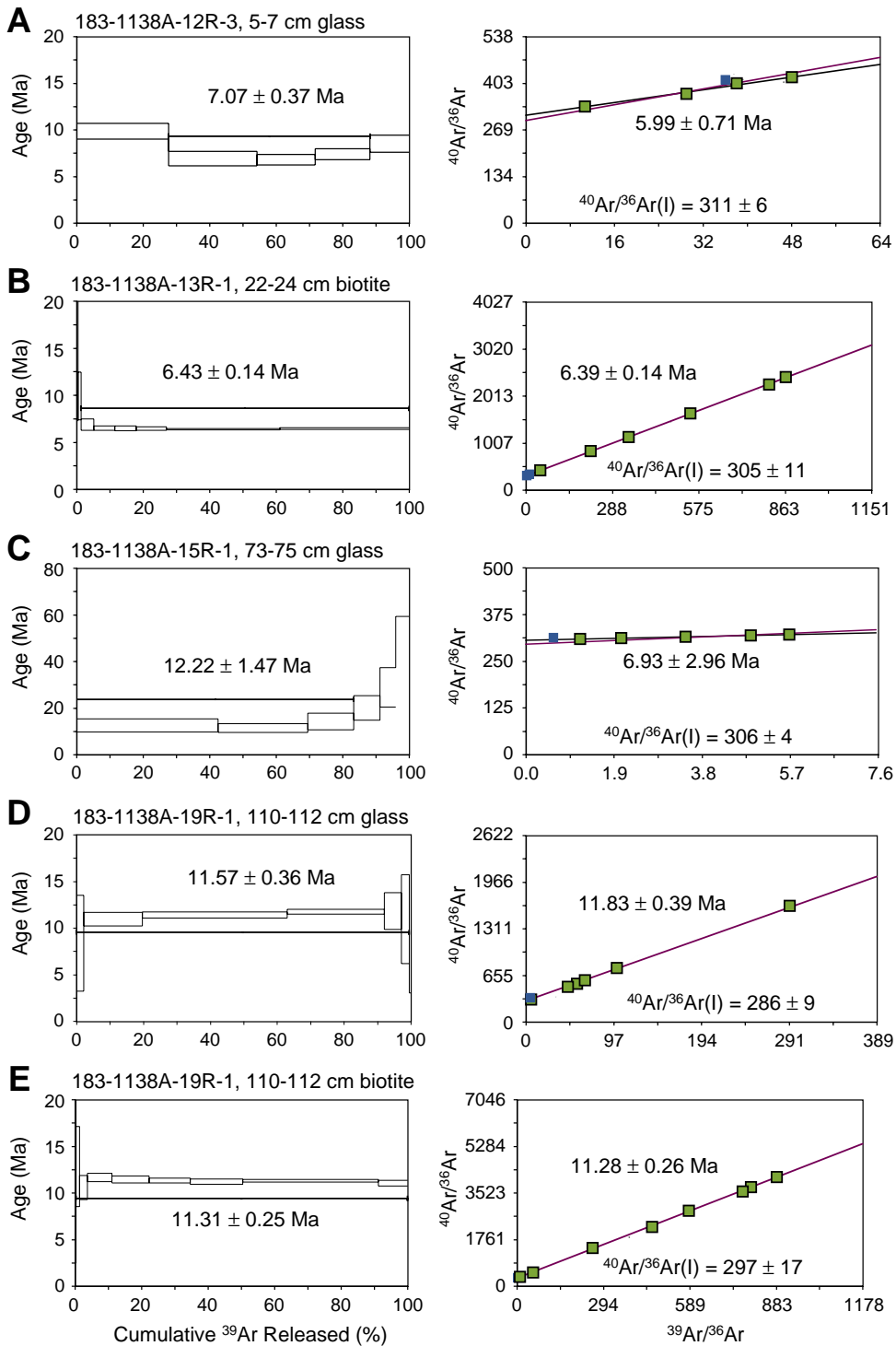
Figure F6. Age-depth plot for the Neogene section of ODP Hole 1138A. Arrows pointing left = first occurrence datums, arrows pointing right = last occurrence datums. Pink crosses = magnetostratigraphic tie points. Paleomagnetic inclination data are from Coffin, Frey, Wallace, et al. (2000).
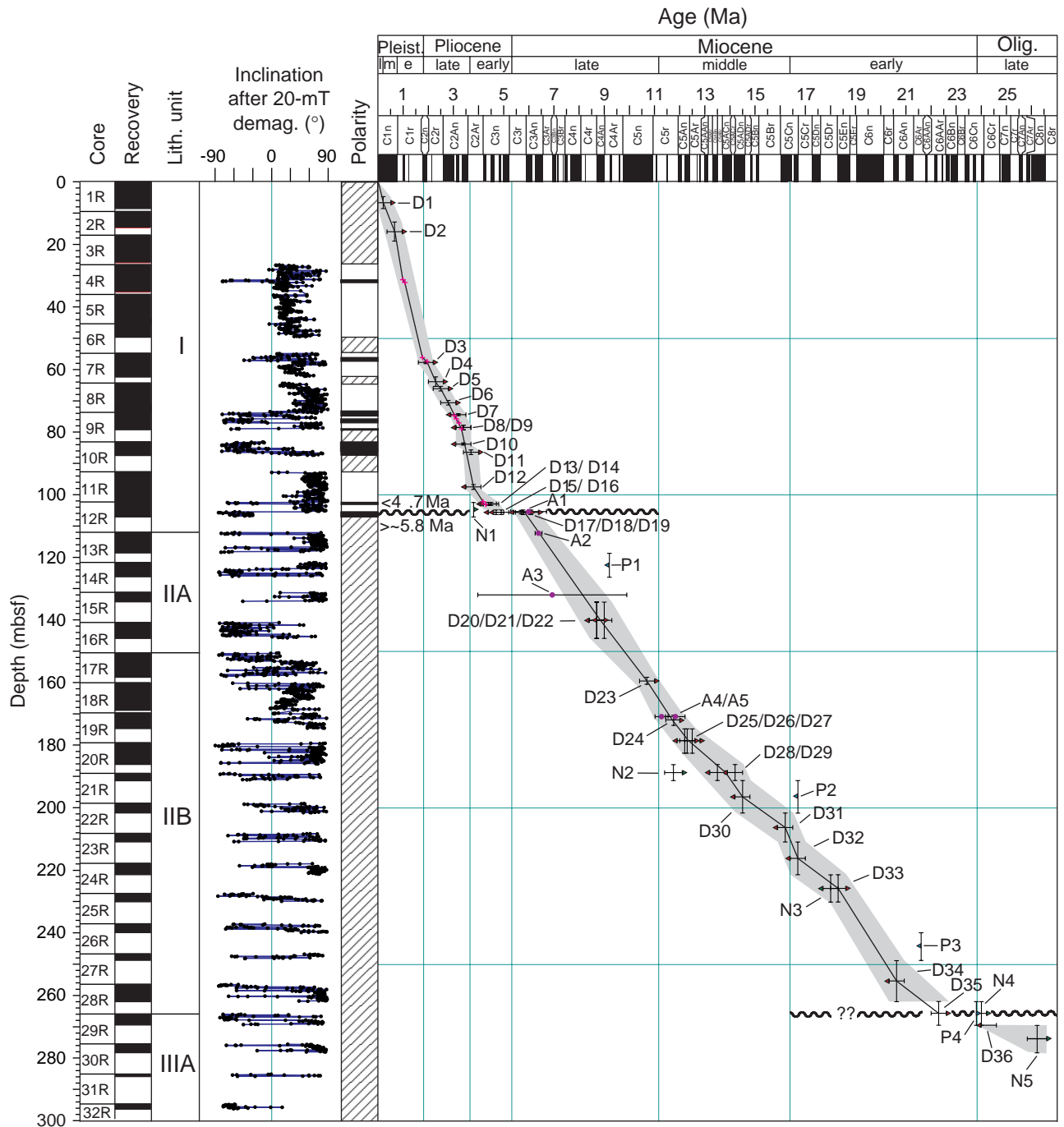
Figure F7. Correlation of middle Miocene tephra horizons from ODP Holes 747A and 1138A. Red bars in core recovery columns = position of tephra horizons (Morche et al., 1992; Coffin, Frey, Wallace, et al., 2000). Hole 747A diatom and magnetostratigraphic data are compiled from Harwood and Maruyama (1992), Harwood et al. (1992), Heider et al. (1992), and Ramsay and Baldauf (1999). Magnetostratigraphy for Hole 747A is interpreted from inclination data presented in Heider et al. (1992). LCAD = last common abundant datum, LO = last occurrence, FO = first occurrence.

Table T1. Relative abundance of diatoms, ebridians, and endoskeletal dinoflagellates in the Neogene, Hole 1138A. (This table is available in an **oversized format.**)

Table T2. Diatom zonal assignments and datums applied to the Miocene, Hole 1138A.

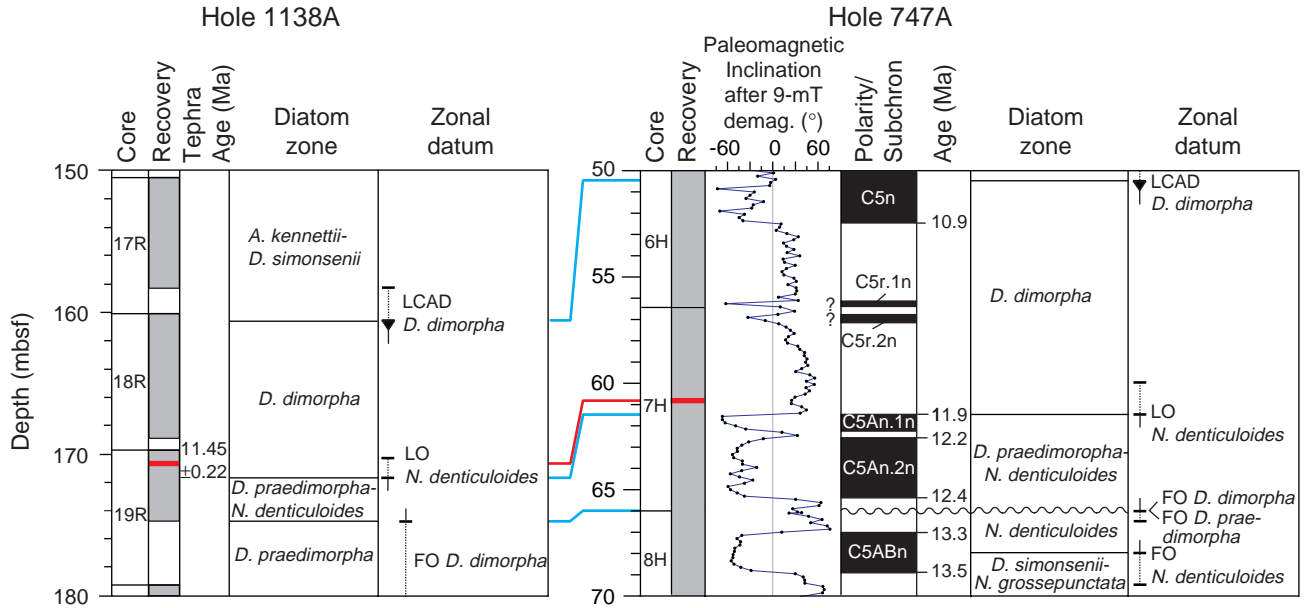| Core, section, interval (cm)	Depth (mbsf)	Diatom zone	Lower datum		Upper datum		Time-rock unit
			Event	Age (Ma)	Event	Age (Ma)	
183-1138A-							
12R-3, 100–101	106.30						
12R-CC, 23–28	107.03						
13R-1, 100–101	113.00	*Nitzschia reinholdii*	FO *Thalassiosira oliverana*	6.4	FO *Thalassiosira tetraoestrupii* group	5.7	
13R-2, 100–101	114.50						
13R-3, 100–101	116.00						
13R-4, 100–101	117.50						
13R-CC, 19–24	118.59						
14R-1, 52–53	122.12						
14R-2, 50–51	123.60	*Actinocyclus ingens* var. *ovalis*	FO *Actinocyclus ingens* var. *ovalis*	8.7	FO *Thalassiosira oliverana*	6.4	upper Miocene
14R-3, 50–51	125.10						
15R-CC, 15–20	134.23						
16R-CC, 13–18	145.85						
17R-2, 50–51	152.50	*Asteromphalus kennettii/Denticulopsis simonsenii*	LCO *Denticulopsis dimorpha*	10.7	FO *Thalassiosira torokina*	9.0	
17R-4, 50–51	155.50						
17R-CC, 5–10	158.27						
18R-1, 50–51	160.60						
18R-2, 50–51	162.10						
18R-3, 50–51	163.60						
18R-4, 50–51	165.10	*Denticulopsis dimorpha*	LO *Nitzschia denticuloides*	11.75	LCO *Denticulopsis dimorpha*	10.7	
18R-5, 50–51	166.60						
18R-6, 50–51	168.10						
18R-CC, 0–7	168.84						
19R-1, 50–51	170.20						
19R-2, 50–51	171.70						
19R-3, 50–51	173.20	*Denticulopsis praedimorpha–Nitzschia denticuloides*	FO *Denticulopsis dimorpha*	12.2	LO *Nitzschia denticuloides*	11.75	middle Miocene
19R-CC, 15–20	174.75						
20R-2, 50–51	181.30	*Denticulopsis praedimorpha*	FO *Denticulopsis praedimorpha*	12.8	FO *Denticulopsis dimorpha*	12.2	
20R-4, 50–51	184.30						
20R-CC, 12–17	186.14	*Nitzschia denticuloides*	FO *Nitzschia denticuloides*	13.5	FO *Denticulopsis praedimorpha*	12.8	
21R-CC, 15–20	191.26	*Actinocyclus ingens* var. *nodus*	FO *Actinocyclus ingens* var. *nodus*	14.5	FO *Denticulopsis simonsenii*	14.2	
22R-CC, 0–5	201.60	*Nitzschia grossepunctata/Actinocyclus ingens–Denticulopsis maccollumii*	FCO *Actinocyclus ingens*	16.2	FO *Actinocyclus ingens* var. *nodus*	14.5	
23R-CC	210.85	*Denticulopsis maccollumii*	FO *Denticulopsis maccollumii*	16.7	FCO *Actinocyclus ingens*	16.2	
24R-CC, 11–16	221.34	*Crucidenticula kanayae/Thalassiosira praefraga* "c"	LO *Thalassiosira praefraga*	18.3	FO *Denticulopsis maccollumii*	16.7	
25R-CC, 12–17	230.02						
26R-CC, 0–5	239.85	*Thalassiosira praefraga* "a–b"	FO *Thalassiosira praefraga*	20.8	LO *Thalassiosira praefraga*	18.3	
27R-CC, 0–5	248.71						
28R-CC, 0–10	261.81	*Thalassiosira spumellaroides*	LO *Rocella gelida*	22.3	FO *Thalassiosira praefraga*	20.8	
29R-CC, 8–13	269.41	*Rocella gelida* "c"	LO *Lisitzinia ornata* (absent)	24.3	LO *Rocella gelida*	22.3	lower Miocene
30R-CC, 14–19	278.21						
31R-CC, 0–10	285.85						
32R-CC, 14–19	296.30						
34R-CC	319.23	Not zoned					
35R-CC, 12–17	330.78						
36R-CC, 0–5	340.60						

Notes: Ages are compiled from the sources listed in Table T5, p. 48, and are revised to the Berggren et al. (1995) timescale. LO = last occurrence, FO = first occurrence, FCO = first common occurrence, LCO = last common occurrence.

Table T3. Diatom zonal assignments and datums applied to the Pliocene–Pleistocene, Hole 1138A. (**See table notes.** Continued on next page.)

Core, section, interval (cm)	Depth (mbsf)	Diatom zone	Lower datum		Upper datum		Time-rock unit
			Event	Age (Ma)	Event	Age (Ma)	
183-1138A-							
1R-1, 70–71	0.70						
1R-2, 109–110	2.59						
1R-3, 69–70	3.69	*Thalassiosira lentiginosa*	LO *Actinocyclus ingens*	0.66	LO *Thalassiosira lentiginosa*	0.0	
1R-4, 20–21	4.70						
1R-CC, 16–21	8.53						
2R-CC, 7–12	12.78						
3R-2, 34–35	18.94						
3R-CC, 7–12	25.57						
4R-1, 25–26	26.75						
4R-CC, 6–11	34.94						
5R-1, 100–101	37.00						
5R-2, 25–26	37.75						
5R-2, 100–101	38.50						Pleistocene
5R-3, 100–101	40.00	*Actinocyclus ingens*	LO *Fragilariopsis barronii*	1.4	LO *Actinocyclus ingens*	0.66	
5R-4, 100–101	41.50						
5R-5, 100–101	43.00						
5R-6, 100–101	44.50						
5R-7, 25–26	45.25						
5R-CC, 12–17	45.58						
6R-1, 100–101	46.40						
6R-2, 100–101	47.90						
6R-3, 100–101	49.40						
6R-CC, 12–17	49.65	*Fragilariopsis kerguelensis*	LO *Thalassiosira kolbei*	1.9	LO *Fragilariopsis barronii*	1.4	
7R-1, 100–101	55.80						
7R-2, 100–101	57.30						
7R-3, 25–26	58.05						
7R-3, 100–101	58.80						
7R-4, 100–101	60.30	*Thalassiosira kolbei*	LO *Thalassiosira vulnifica*	2.3	LO *Thalassiosira kolbei*	1.9	
7R-5, 100–101	61.80						
7R-CC, 13–18	62.31						
8R-1, 100–101	65.30						
8R-2, 100–101	66.80	*Thalassiosira vulnifica*	LO *Thalassiosiraceae insigna*	2.6	LO *Thalassiosira vulnifica*	2.3	upper Pliocene
8R-3, 100–101	68.30						
8R-4, 100–101	69.80						
8R-5, 100–101	71.30	*Thalassiosira insigna–Thalassiosira vulnifica*	FO *Thalassiosira vulnifica*	3.2	LO *Thalassiosira insigna*	2.6	
8R-6, 100–101	72.80						
8R-CC, 10–15	74.04						
9R-1, 100–101	74.70						
9R-2, 100–101	76.20						
9R-3, 100–101	77.70						
9R-CC, 14–19	79.21						
10R-1, 25–26	83.35						
10R-1, 100–101	84.10	*Fragilariopsis interfrigidaria*	FO *Fragilariopsis interfrigidaria*	3.8	FO *Thalassiosira vulnifica*	3.2	
10R-2, 25–26	84.85						
10R-2, 100–101	85.60						lower Pliocene
10R-3, 100–101	87.10						
10R-CC, 13–18	87.53						
11R-1, 100–101	93.70						

Table T3 (continued).

Core, section, interval (cm)	Depth (mbsf)	Diatom zone	Lower datum		Upper datum		Time-rock unit
			Event	Age (Ma)	Event	Age (Ma)	
11R-2, 100–101	95.20						
11R-3, 100–101	96.70						
11R-4, 100–101	98.20						
11R-5, 100–101	99.70	*Fragilariopsis barronii*	FO *Fragilariopsis barronii*	4.4	FO *Fragilariopsis interfrigidaria*	3.8	lower Pliocene
11R-6, 100–101	101.20						
11R-CC, 9–14	102.39						
12R-1, 100–101	103.30	*Thalassiosira inura*	FCO *Thalassiosira inura*	4.9	FO *Fragilariopsis barronii*	4.4	
12R-2, 100–101	104.80						

Notes: Ages are compiled from the sources listed in Table T5, p. 48, and are revised to the Berggren et al. (1995) timescale. LO = last occurrence, FO = first occurrence, FCO = first common occurrence, LCO = last common occurrence.

Table T4. ^{40}Ar-^{39}Ar incremental heating ages from ash layers in the Neogene, Hole 1138A.

Core, section, interval (cm)	Designation	Depth (mbsf)			Material	Total gas age (Ma)	±2 sd	^{39}Ar (%)	Plateau age (Ma)	±2 sd	Steps used	MSWD	Isochron age (Ma)	±2 sd	MSWD	^{40}Ar/^{36}Ar (initial)	±2 sd
		Top	Bottom	Average													
183-1138A-																	
12R-3, 5–7	A1	105.35	105.37	105.36	Glass	7.98	0.39	60.80	7.07	0.37	3 of 5	1.10	**5.99**	**0.71**	1.34	311	6
13R-1, 22–24	A2	112.22	112.24	112.23	Biotite	6.53	0.14	98.70	**6.43**	**0.14**	6 of 7	1.15	**6.39**	**0.14**	1.15	305	11
15R-1, 73–75	A3	131.93	131.95	131.94	Glass	16.47	1.68	83.30	12.22	1.47	3 of 6	1.02	**6.93**	**2.96**	0.02	306	4
19R-1, 110–112	A4	170.80	170.82	170.81	Biotite	11.32	0.25	99.70	**11.31**	**0.25**	8 of 8	1.24	**11.28**	**0.26**	1.24	297	17
19R-1, 110–112	A5	170.80	170.82	170.81	Glass	11.44	0.39	99.50	**11.57**	**0.36**	6 of 7	1.53	**11.83**	**0.39**	1.53	286	9

Notes: MSWD = mean square weighted deviation. All ages calculated relative to neutron fluence monitor FCT-2 biotite (28.04 ± 0.12 Ma), decay and abundance constants le = 0.581 × 10^{-10}/yr; lb = 4.961 × 10^{-10}/yr; ^{40}K/K = 1.17 × 10^{-4}, and corrected for ^{37}Ar decay (half-life = 35.1 days) and interfering isotopes ^{36}Ar/^{37}Ar[Ca] = 2.64 × 10^{-4}, ^{39}Ar/^{37}Ar[Ca] = 6.73 × 10^{-4}, ^{40}Ar/^{39}Ar[K] = 1.0 × 10^{-3}. Bold entries are considered the best estimates of crystallization ages (see text).

Table T5. Neogene biostratigraphy datums used to construct an age model.

Designation	Taxon	Level (mbsf) Present	Level (mbsf) Absent	Age (Ma)	Source(s)
Diatoms					
D1	LCO *Hemidiscus karstenii*	8.53	4.70	0.18–0.21	Bu, ZG
D2	LCO *Actinocyclus ingens*	18.94	12.78	0.64–0.70	C, G, HM, GB, ZG
D3	LO *Thalassiosira kolbei*	58.05	57.30	1.9–2.0	G, HM, W, ZG
D4	LO *Thalassiosira vulnifica*	65.30	62.31	2.3–2.4	C, BB, ZG
D5	LO *Thalassiosira lentiginosa* var. *ovalis*	66.80	65.30	2.5	C, HM
D6	LO *Fragilariopsis weaveri*	71.30	69.80	2.8	C
D7	FO *Thalassiosira vulnifica*	74.04	74.70	3.2	C, W, HM
D8	FO *Thalassiosira insigna*	77.70	79.21	3.4	HM, ZG
D9	FO *Thalassiosira lentiginosa* var. *ovalis*	77.70	79.21	3.4	HM
D10	FO *Fragilariopsis weaveri*	83.35	84.10	3.4	BB, HM, ZG
D11	LO *Fragilariopsis praeinterfrigidaria*	87.10	85.60	3.7	HM
D12	FO *Fragilariopsis interfrigidaria*	96.70	98.20	3.8	G, BB, HM, ZG
D13	FO *Fragilariopsis barronii*	102.39	103.30	4.2–4.6	C, G, BB, HM
D14	FO *Thalassiosira striata*	102.39	103.30	4.5	HM
D15	FO *Thalassiosira complicata*	104.80	106.30	4.7	G, HM
D16	FCO *Thalassiosira inura*	104.80	106.30	4.9	G, HM
D17	FO *Thalassiosira tetraoestrupii* group	104.80	106.30	5.6–5.8	BB, HM
D18	LO *Fragilariopsis donahuensis*	106.30	104.80	5.8	HM
D19	LO *Nitzschia miocenica*	106.30	104.80	6.0–6.2	B, BB, BI
D20	LO *Denticulopsis crassa*	145.85	134.23	8.7	WI (CG = 7.5 Ma)
D21	FO *Actinocyclus ingens* var. *ovalis*	134.23	145.85	8.7	G, HM, CG
D22	FO *Thalassiosira torokina*	134.23	145.85	9.0	HM
D23	LCO *Dentculopsis dimorpha* var. *areolata*	160.60	158.27	10.7	HM
D24	LO *Nitzschia denticuloides*	171.70	170.20	11.7–11.8	HM, CG
D25	FO *Dentculopsis dimorpha* var. *areolata*	174.75	181.30	12.2	BB, HM
D26	LO *Crucidenticula nicobarica*	181.30	174.75	12.3	BB, HM
D27	LO *Actinocyclus ingens* var. *nodus*	181.30	174.75	12.5	G, HM
D28	FO *Nitzschia denticuloides*	186.14	191.26	13.5	G, CG
D29	FO *Denticulopsis simonsenii*	186.14	191.26	14.2	G, BB, HM, CG
D30	FO *Actinocyclus ingens* var. *nodus*	191.26	201.60	14.5	HM, CG
D31	FCO *Actinocyclus ingens*	201.60	210.85	16.2	BB, HM, CG
D32	FO *Denticulopsis maccollumii*	210.85	221.34	16.7	HM, CG
D33	LO *Thalassiosira praefraga*	230.02	221.34	18.3	HM
D34	FO *Thalassiosira praefraga*	248.71	261.81	20.3–20.8	HM, YA
D35	LO *Rocella gelida*	269.41	261.81	22.3	BB, HM
D36	LO *Lisitzinia ornata* (absent)	—	269.41	<24.3	HM
Calcareous nannofossils					
N1	LO *Reticulofenestra perplexa*	107.03	102.39	3.8	183 IR
N2	LO *Cyclicargolithus floridanus floridanus*	191.26	186.14	11.4–12.1	183 IR
N3	FO *Calcidiscus leptoporus/macintyrei*	221.34	230.02	17.7–18.3	183 IR
N4	LO *Reticulofenestra bisecta*	269.41	261.81	23.8–24.2	183 IR
N5	LO *Chiasmolithus altus*	278.21	269.41	25.8–26.6	183 IR
Planktonic foraminifers					
P1	FO *Neogloboquadrina pachyderma*	118.59	126.23	9.2	183 IR
P2	FO *Globorotalia miozea*	191.26	201.60	16.7	183 IR
P3	FO *Paragloborotalia incognita*	239.85	248.71	21.6	183 IR
P4	LO *Globigerina euapertura*	269.41	261.81	23.8	183 IR

Notes: The age model is presented in Figure F6, p. 41. All diatom ages are calibrated to the Berggren et al. (1995) timescale and are compiled from the following sources: Bu = Burckle et al. (1978), C = Ciesielski (1983), B = Baldauf (1985), G = Gersonde and Burckle (1990), BB = Baldauf and Barron (1991), HM = Harwood and Maruyama (1992), BI = Baldauf and Iwai (1995), W = Winter and Harwood (1997), GB = Gersonde and Bárcena (1998), YA = Yanagisawa and Akiba (1998), RB = Ramsay and Baldauf (1999), WI = Winter and Iwai (2002), ZG = Zielinski and Gersonde (2002), and CG = Censarek and Gersonde (2002). Planktonic foraminifer and nannofossil datums are compiled from the Leg 183 *Initial Reports* volume (Coffin, Frey, Wallace, et al., 2000). LO = last occurrence, LCO = last common occurrence, FO = first occurrence, and FCO = first common occurrence.

Table T6. Interpreted paleomagnetic stratigraphy and ages for the Pliocene–Pleistocene, Hole 1138A.

Reversal	Depth (mbsf)	Age (Ma)
T C1r.1n	31.32	0.99
B C1r.1n	31.95	1.07
T C2n	55.85	1.77
B C2n	57.10	1.95
B C2An.1n	74.83	3.04
T C2An.2n	75.67	3.11
B C2An.2n	77.02	3.22
T C2An.3n	78.82	3.33
T C3n.1n	102.42	4.18
B C3n.1n	102.87	4.29

Notes: Ages are from Berggren et al., 1995. T = top, B = bottom.

Plate P1. All specimens are at the same scale. **1.** *Thalassiosira bipora* Shiono (Sample 183-1138A-8R-5, 100–101 cm). **2, 3.** *Actinocyclus ingens* var. *ovalis* Gersonde (Sample 183-1138A-15R-CC). **4.** *Thalassiosira insigna* (Jousé) Harwood and Maruyama (Sample 183-1138A-8R-CC). **5.** *Thalassiosira* sp. 1 (this study). Arrow denotes position of prominent strutted process located between valve center and margin (Sample 183-1138A-7R-1, 100–101 cm). **6.** *Thalassiosira* sp. cf. *T. eccentrica* (Ehrenberg) Cleve (high and low focus) (Sample 183-1138A-15R-CC). **7, 12.** *Actinocyclus ingens* var. 1 (this study) (Sample 183-1138A-23R-CC). **8, 9.** *Actinocyclus ingens* var. 2 (this study) (Sample 183-1138A-4R-1, 25–26 cm). **10.** *Azpeitia harwoodii* Bohaty and Shiono n. sp. (Sample 183-1138A-11R-CC). **11.** *Actinocyclus dimorphus* (Castracane) Harwood and Maruyama (Sample 183-1138A-8R-CC).
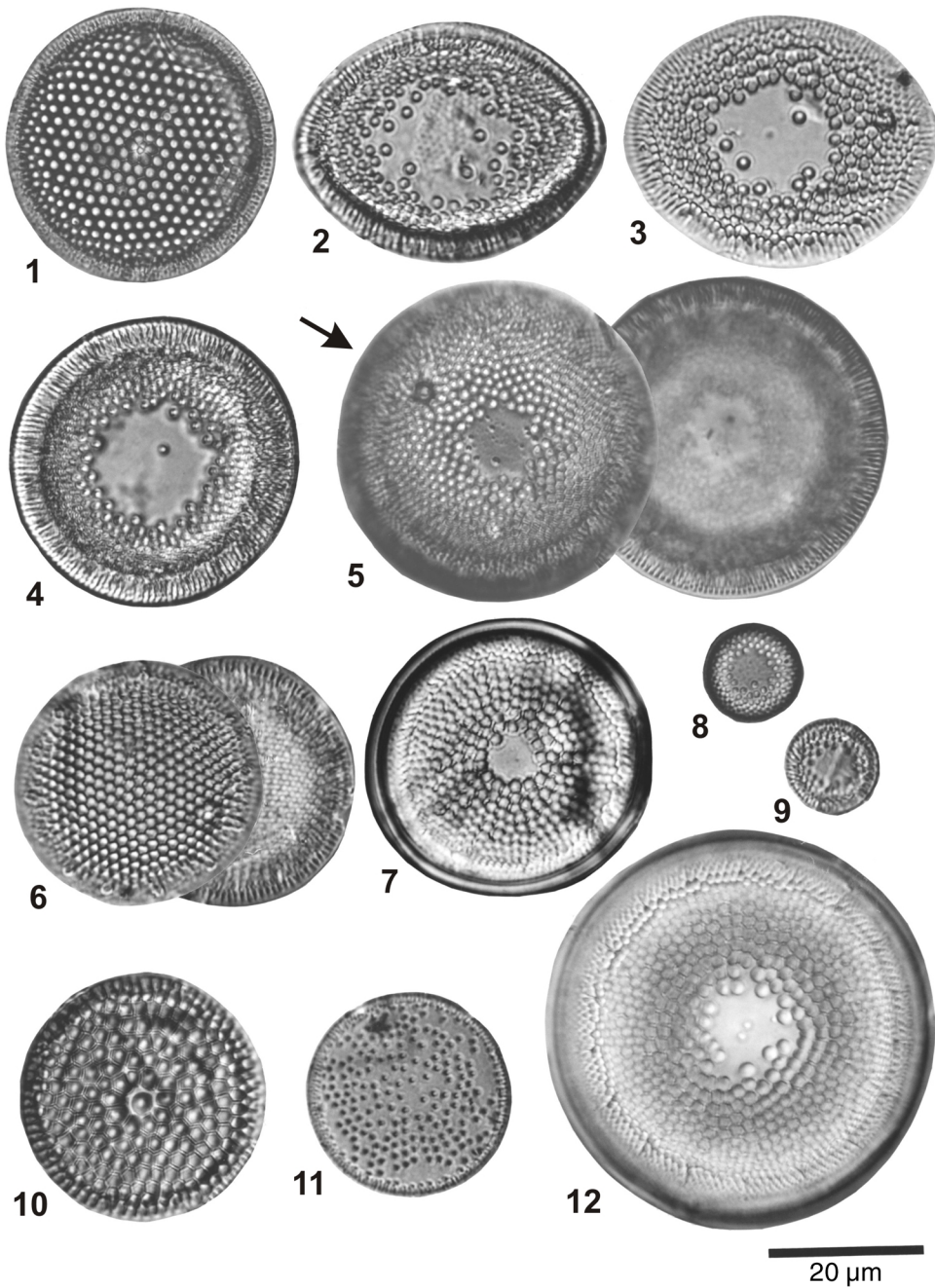

1

2

3

4

5

6

7

8

9

10

11

12

20 μm

Plate P2. All specimens are at the same scale. **1–7.** *Fragilariopsis heardensis* Bohaty n. sp.; (1a, 1b) holotype (Sample 183-1138A-8R-5, 100–101 cm); (2, 3) Sample 183-1138A-8R-CC; (4–7) Sample 183-1138A-8R-5, 100–101 cm. **8, 9.** *Fragilariopsis clementia* (Gombos) Zielinski and Gersonde (Sample 183-1138A-12R-1, 100–101 cm). **10, 11.** *Fragilariopsis lacrima* (Gersonde) Gersonde and Bárcena (Sample 120-751A-4H-4, 70 cm). **12.** *Synedropsis* sp. B (this study) (Sample 183-1138A-8R-5, 100–101 cm). **13.** *Fragilariopsis kerguelensis* (O'Meara) Hustedt, "early" form (Sample 183-1138A-4R-1, 25–26 cm). **14.** *Rouxia* sp. 1 (this study) (Sample 183-1138A-8R-CC). **15–18.** *Fragilariopsis interfrigidaria* (McCollum) Gersonde and Bárcena; (15–17) Sample 183-1138A-10R-CC; (18) Sample 183-1138A-8R-5, 100–101 cm. **19.** *Entopyla* sp. (Sample 183-1138A-8R-5, 100–101 cm).
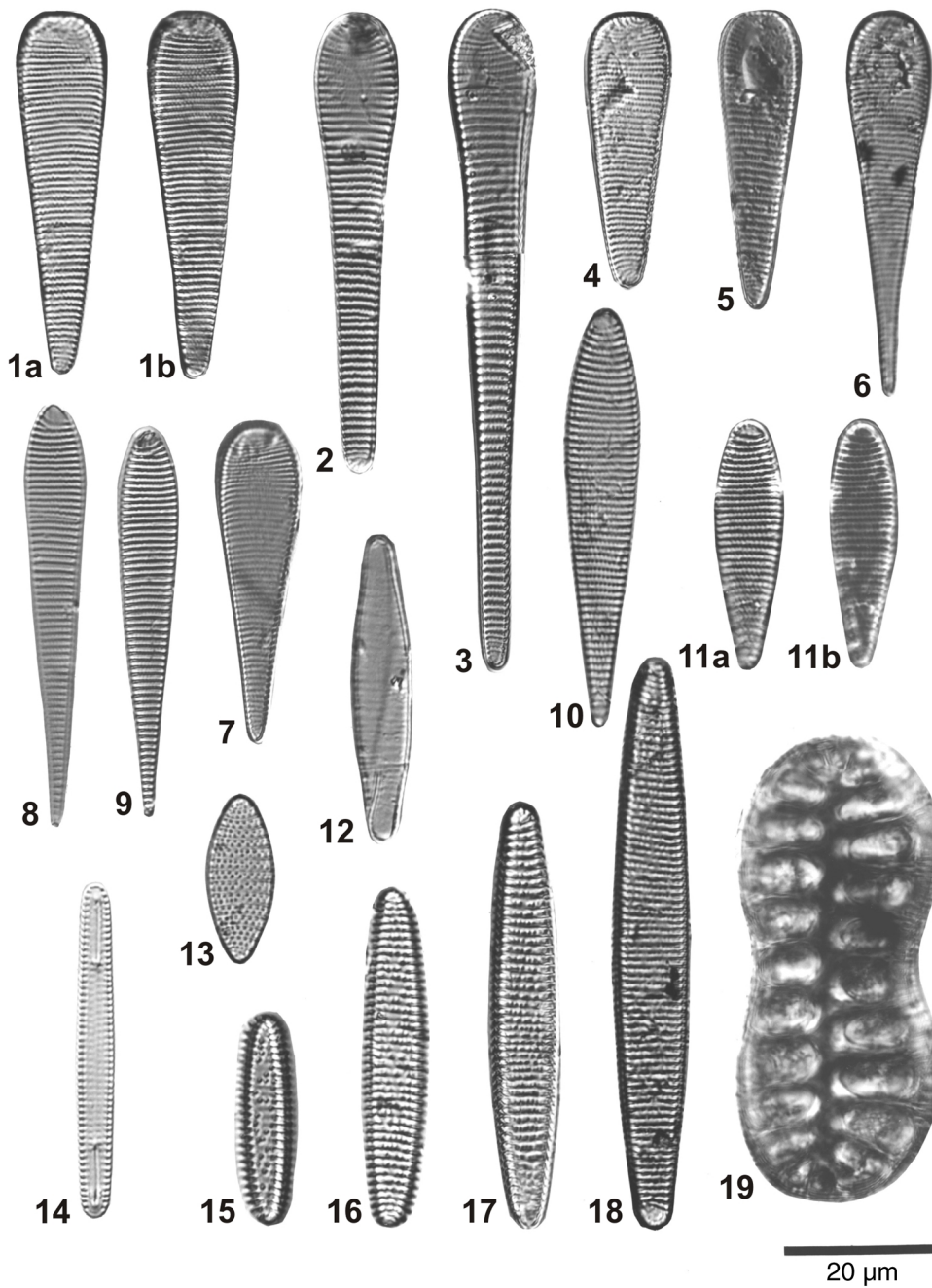
Plate P3. Figures 1–9 at the same scale. **1–6, 10–13.** *Azpeitia harwoodii* Bohaty and Shiono n. sp. (Sample 183-1138A-11R-6, 100–101 cm); (1) holotype (high and low focus); (3–6) high and low focus; (10) diameter = 18 μm; (11) diameter = 26 μm; (12) diameter = 24 μm; (13) diameter = 28 μm. **7, 8.** *Rouxia* sp. 1 (this study) (Sample 183-1138A-8R-CC). **9.** *Fragilariopsis heardensis* Bohaty n. sp. (Sample 183-1138A-8R-CC).
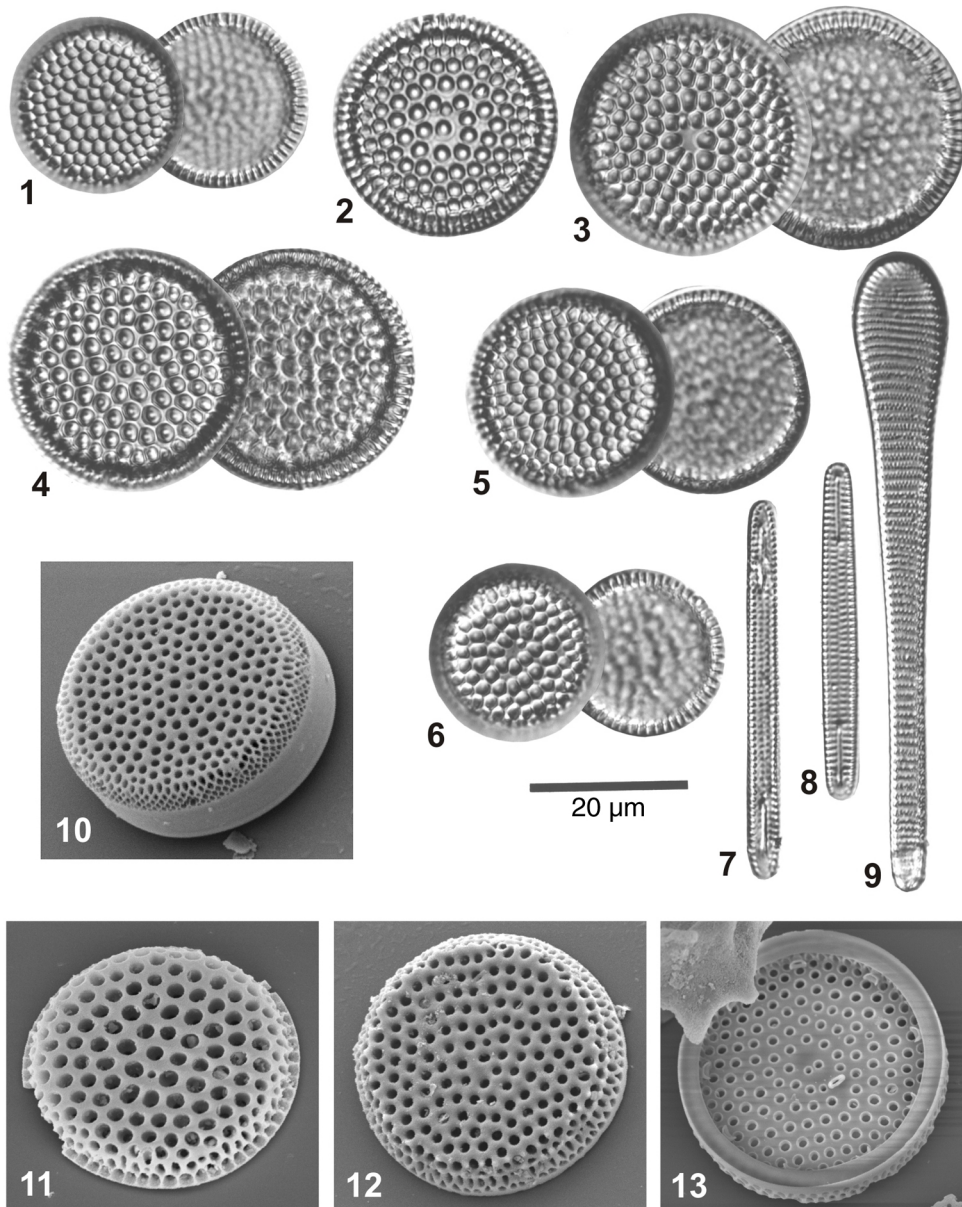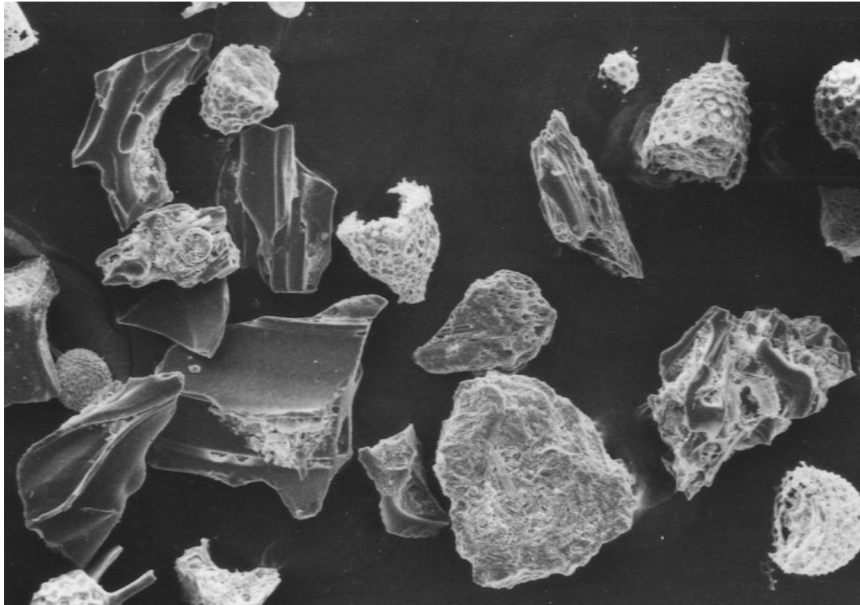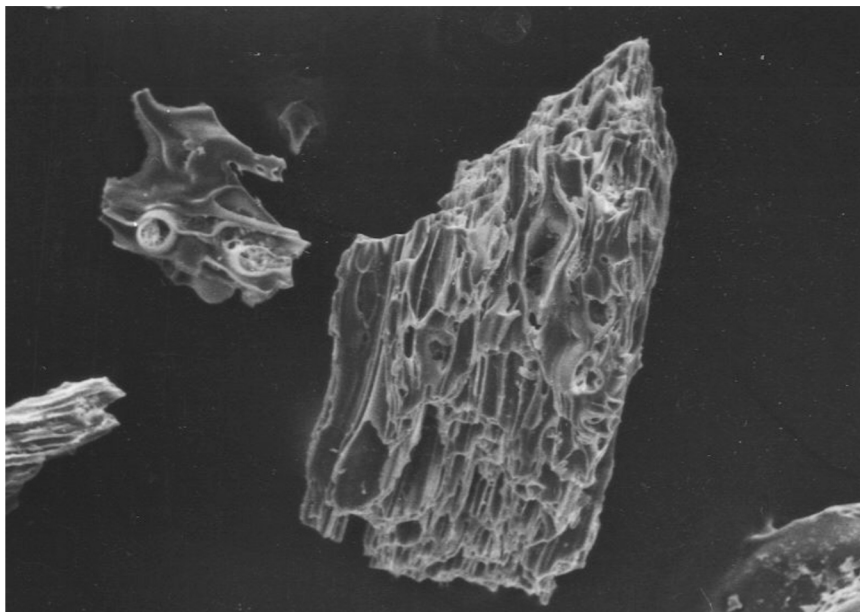
Plate P4. SEM photographs of glass shards contained in tephra layers recovered from Hole 1138A. **1.** Sample 183-1138A-12R-3, 5–7 cm. **2.** Sample 183-1138A-15R-1, 73–75 cm.

1   200 µm

2   200 µm